THE PROTEIN SOCIETY

Design and characterization of ebolavirus GP prehairpin intermediate mimics as drug targets

Tracy R. Clinton,[1] Matthew T. Weinstock,[1] Michael T. Jacobsen,[1] Nicolas Szabo-Fresnais,[1,2] Maya J. Pandya,[1] Frank G. Whitby,[1] Andrew S. Herbert,[3] Laura I. Prugar,[3] Rena McKinnon,[4] Christopher P. Hill,[1] Brett D. Welch,[4] John M. Dye,[3] Debra M. Eckert,[1]* and Michael S. Kay[1]*

[1]Department of Biochemistry, University of Utah School of Medicine, Salt Lake City, Utah 84112-5650
[2]Cardiology Section, Department of Internal Medicine, University of Utah School of Medicine, Salt Lake City, Utah 84148
[3]U.S. Army Medical Research Institute of Infectious Diseases, Fort Detrick, Frederick, Maryland 21702-5011
[4]D-Peptide Research Division, Navigen, Inc., Salt Lake City, Utah 84108

Received 21 August 2014; Accepted 1 October 2014
DOI: 10.1002/pro.2578
Published online 00 Month 2014 proteinscience.org

Abstract: Ebolaviruses are highly lethal filoviruses that cause hemorrhagic fever in humans and non-human primates. With no approved treatments or preventatives, the development of an anti-ebolavirus therapy to protect against natural infections and potential weaponization is an urgent global health need. Here, we describe the design, biophysical characterization, and validation of peptide mimics of the ebolavirus N-trimer, a highly conserved region of the GP2 fusion protein, to be used as targets to develop broad-spectrum inhibitors of ebolavirus entry. The N-trimer region of GP2 is 90% identical across all ebolavirus species and forms a critical part of the prehairpin intermediate that is exposed during viral entry. Specifically, we fused designed coiled coils to the N-trimer to present it as a soluble trimeric coiled coil as it appears during membrane fusion. Circular dichroism, sedimentation equilibrium, and X-ray crystallography analyses reveal the helical, trimeric structure of the designed N-trimer mimic targets. Surface plasmon resonance studies validate that the N-trimer mimic binds its native ligand, the C-peptide region of GP2. The longest N-trimer mimic also inhibits virus entry, thereby confirming binding of the C-peptide region during viral entry and the presence of a vulnerable prehairpin intermediate. Using phage display as a model system, we validate the suitability of the N-trimer mimics as drug screening targets. Finally, we describe the foundational work to use the N-trimer mimics as targets in mirror-image phage display, which will be used to identify D-peptide inhibitors of ebolavirus entry.

Keywords: ebolavirus; filovirus entry; ebolavirus GP2; prehairpin intermediate; designed coiled coil; N-trimer; phage display; mirror-image phage display

Additional Supporting Information may be found in the online version of this article.

Disclosure: D.M.E., B.D.W. and M.S.K. are Scientific Directors and equity holders of the D-Peptide Research Division of Navigen, which is commercializing D-peptide inhibitors of viral entry. D.M.E. and M.S.K. are also Navigen consultants.

Matthew T. Weinstock current address is Synthetic Genomics, Inc., La Jolla, California 92037

*Correspondence to: Debra M. Eckert; Department of Biochemistry, University of Utah School of Medicine, 15 N. Medical Drive East, Rm 4100, Salt Lake City, UT 84112. E-mail: deckert@biochem.utah.edu or Michael S. Kay; Department of Biochemistry, University of Utah School of Medicine, 15 N. Medical Drive East, Rm 4100, Salt Lake City, UT 84112. E-mail: kay@biochem.utah.edu

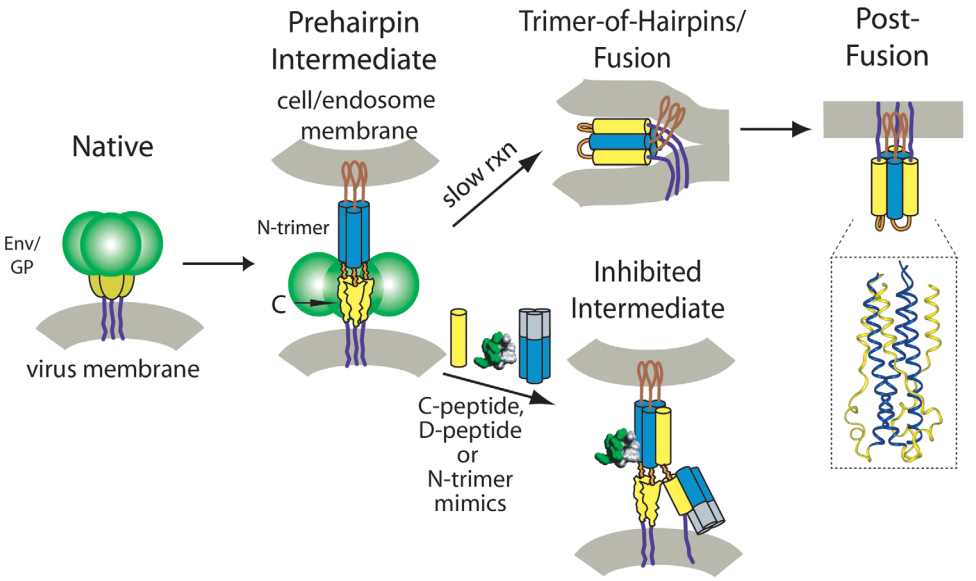

Figure 1. Model for membrane fusion mediated by enveloped virus surface glycoproteins. The HIV-1 and ebolavirus entry events are predicted to be similar. First, the surface glycoprotein (Env for HIV-1, GP for ebolavirus) facilitates viral attachment to the cell and, for ebolavirus, the virus is endocytosed and then cleaved by endosomal proteases. Engagement of the virus receptors (CD4 and a chemokine receptor for HIV-1, NPC1 for ebolavirus) is followed by a conformational change in Env/GP, and insertion of the fusion peptide/loop (brown) into the host cell membrane. At this stage, the virus is in a transient state that bridges both membranes, termed the "prehairpin intermediate," which is vulnerable to inhibition. In the absence of an inhibitor, the Env/GP structure slowly resolves into the highly stable trimer-of-hairpins structure, juxtaposing the two membranes, and leading to membrane fusion. The inset shows the high resolution structure of the ebolavirus trimer-of-hairpins (PDB: 2EBO).[27] In HIV, it has been shown that inhibitors that bind to either the N-trimer (blue) or C-peptide (yellow) regions are capable of inhibiting entry [as reviewed in Ref. (17)].

Introduction

Ebolaviruses are enveloped, negative-strand RNA viruses that cause severe hemorrhagic fever.[1] Since its identification in 1976, there have been over 20 reported natural ebolavirus outbreaks, the majority since 2000, and several accidental laboratory exposures with an overall mortality rate >60%.[2] Alarmingly, in 2014 the largest known outbreak is occurring in western Africa[3] and has crossed international borders. Currently, no vaccines or therapeutics are FDA approved. Because of ease of transmission, high mortality, and potential for a severe impact on public health, the CDC places ebolaviruses in its highest category of potential agents of bioterrorism.[4] There is a vital need for preventatives and/or therapeutics to protect against future natural, accidental, or deliberate outbreaks.

Ebolavirus entry into host cells, a critical step to infection, is mediated by the viral surface glycoprotein (GP), a class I fusion protein.[5] GP comprises two disulfide-linked subunits, one surface exposed (GP1) and one embedded in the viral membrane (GP2).[6,7] Following binding to host cells via cell surface attachment factors, the virus is endocytosed. Endosomal cysteine proteases, cathepsins B and L, cleave off much of GP1, exposing the binding site for the receptor, endosomal NPC1.[8–12] At this point, the fusion mechanism is thought to mimic that of other well characterized viral class I fusion proteins, such as HIV-1 and influenza[13–15] (Fig. 1). GP2 forms a transient conformation ("prehairpin intermediate") embedded in both the virus (via the transmembrane domain) and host cell (via the fusion loop) membranes. This prehairpin intermediate exposes a trimeric coiled coil, formed by the N-terminal region (N-trimer), and the C-terminal region (C-peptide). Slow collapse of the intermediate into a very stable trimer-of-hairpins structure, with the C-peptide binding into the grooves on the N-trimer, juxtaposes the virus and cell membranes, leading to membrane fusion. In ebolavirus entry, the low pH of the endosome contributes to the stability of the trimer-of-hairpins.[16]

In the case of HIV-1, the prehairpin intermediate has been exploited to develop highly potent viral entry inhibitors (Fig. 1). Peptides and proteins that bind with high affinity to either the N-trimer or C-peptide regions prevent formation of the trimer-of-hairpins, thereby halting viral entry [as reviewed in Ref. (17)]. The most potent of the HIV entry inhibitors, chol-PIE12-trimer, binds to the conserved hydrophobic pockets of the HIV N-trimer and inhibits HIV entry with low picomolar potency.[18] Since filoviruses share a similar mechanism of entry as HIV-1, they are likely vulnerable to inhibitors that similarly target the prehairpin intermediate.

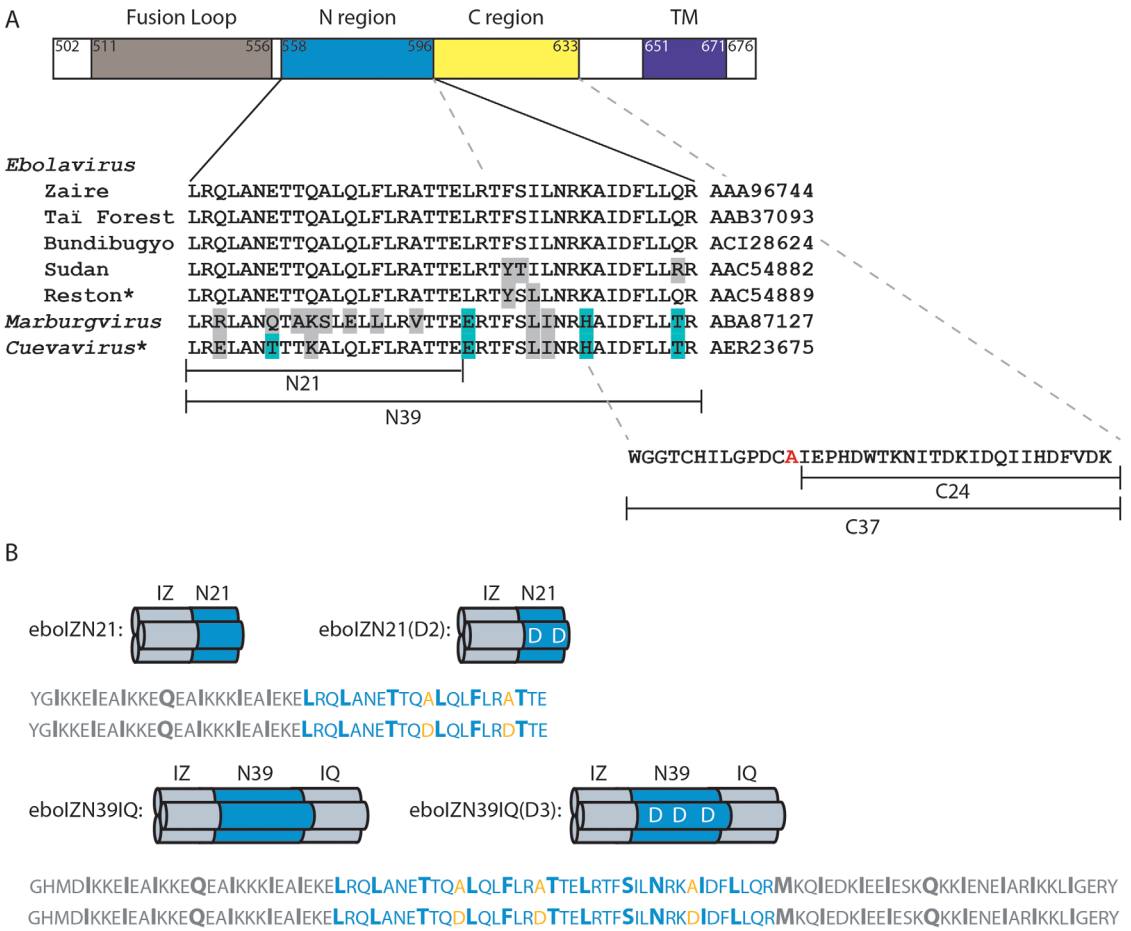

Figure 2. Conservation of the ebolavirus GP N-trimer and design of peptide N-trimer mimics. (A) Schematic of the primary structure of ebolavirus GP2, indicating the fusion loop (brown), N-trimer (blue), C-peptide (yellow), and transmembrane domain (TM, purple), all shown approximately to scale. The sequences of the N-trimer region (residues 558–596) and the C-peptide region (residues 597–633) (*Zaire ebolavirus* species, representative Mayinga strain isolated in Zaire in 1976[60]) contained in the peptides described in this study are indicated. In the C-peptide, cysteine 609, which is proposed to disulfide bond with GP1,[76] is mutated to alanine in our constructs (red). Below the Zaire N-trimer is an alignment of the sequences from the 4 additional ebolavirus species plus Marburgvirus and Cuevavirus filoviruses. Genbank accession codes are indicated (right). Conserved changes (score of 0 or higher in BLOSUM62 matrix[77]) are highlighted in gray, nonconserved in cyan. Notably, 3/5 and 5/5 ebolavirus species are 100% identical in the N39 and N21 regions, respectively. The 2014 epidemic is caused by the *Zaire ebolavirus* species and is 100% identical in this region.[3] *Reston and likely Cuevavirus (Lloviu virus) are not pathogenic to humans. (B) Schematics and sequences of the N-trimer mimics and their corresponding binding site mutants [eboIZN21 and eboIZN21(D2); eboIZN39IQ and eboIZN39IQ(D3)]. The designed coiled coils, IZ_m and IQ, are shown in gray, while the ebolavirus N-trimer is shown in blue. The a and d positions of the coiled-coil heptad repeats are indicated by a larger bolded font, including a stutter at the N-terminal end of the ebolavirus N-trimer as seen in the crystal structures,[27,28] where the coil is underwound, leading to an atypical 3-4-4-3 pattern (instead of the standard 3-4, or a-g, periodicity of a heptad repeat). The alanine residues along the C-peptide binding groove that are mutated to aspartate in the binding site mutants are shown (orange).

There are five known species of ebolavirus, four of which are pathogenic to humans. The vast majority of promising preventative and therapeutic candidates with efficacy against ebolavirus in animal models, such as vaccines, antibodies, and antisense compounds (e.g.,[19–23]), are species-specific, resulting in limited breadth and difficulty in combating emerging species. The N-trimer of the prehairpin intermediate provides a highly conserved target for potential broad-spectrum inhibitors. Indeed, although the overall sequence identity of GP across all known ebolavirus species is only 42%, the N-peptide region is 90% identical, and all changes are conservative [Fig. 2(A)].

Here, we describe the development of ebolavirus N-trimer mimics that will be useful in a variety of drug discovery platforms to screen small molecule, antibody, and peptide libraries for entry inhibitors that target this conserved region. Specifically, we have designed and characterized peptide mimics of ebolavirus N-trimers, validated their use as drug discovery tools, and explored conditions that can be applied directly to phage display drug discovery endeavors. In addition, using one of our N-trimers as an inhibitor itself (to

target the C-peptide region of the prehairpin intermediate), we have confirmed the vulnerability of the ebolavirus GP prehairpin intermediate to entry inhibition.

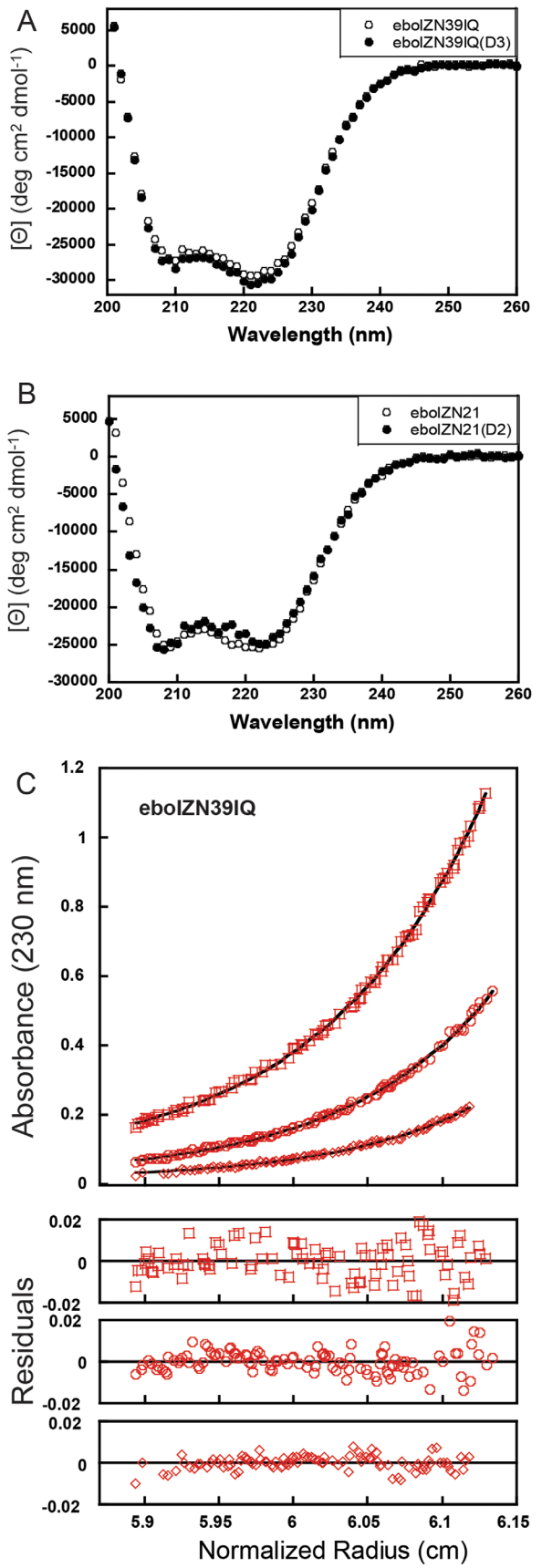

Figure 3. Biophysical analyses of ebolavirus N-trimer mimics. (A) CD spectra of 11.4 μ*M* eboIZN39IQ and 11.1 μ*M* eboIZN39IQ(D3) at 25°C. Both spectra indicate a highly helical conformation with 81 and 83% helicity, respectively. (B) CD spectra of 18.0 μ*M* eboIZN21 and 25.3 μ*M* eboIZN21(D2) at 25°C, also indicate a highly helical conformation with 73 and 71% helicity, respectively. (C) Analytical ultracentrifugation (AUC) sedimentation equilibrium analysis of eboIZN39IQ, shown as representative AUC data. 10, 5, and 2.5 μ*M* peptide solutions were centrifuged at 18,000, 21,000, and 24,000 rpm at 4°C on a Beckman XLA. All data were globally fit to a single ideal species, and an observed molecular weight of 39,762 Da was determined for an M_{obs}/M_{calc} of 3.31. The data (open symbols) and fit (solid lines) are shown for the lowest speed.

Results and Discussion

N-trimer mimic design

Based on our previous HIV-1 work,[24,25] we set out to design soluble peptide mimics of the N-trimer region of the ebolavirus GP prehairpin intermediate by fusing stable, soluble, designed trimeric coiled coils to the N-trimer sequence [Fig. 2(B)]. As with HIV-1, the ebolavirus N-trimer aggregates when produced in isolation. We were interested in presenting the entire N-trimer groove as well as a smaller, more conserved region of the N-trimer to provide flexibility in drug screening. Our initial designs, in which we fused the coiled coil IZ_m(24) to the N-terminus of N-trimer segments of 29 and 39 amino acids, were aggregated as determined by analytical ultracentrifugation (AUC) sedimentation equilibrium experiments (data not shown). To overcome this problem, we fused an additional trimeric coiled coil, GCN4-pI_QI' (IQ)[26] to the C-terminus of the ebolavirus N-trimer segment. The resulting peptide, eboIZN39IQ presents the full ebolavirus N-trimer (determined from available trimer-of-hairpins crystal structures[27,28]) as a trimeric coiled coil, as shown by circular dichroism (CD) [Fig. 3(A)] and AUC [Fig. 3(C) and Table I]. eboIZN39IQ is very stable, as indicated by similar CD spectra at 25, 37, and 50°C (Table I). The ultimate goal for an ebolavirus N-trimer mimic is to use it as a target in drug screening to identify inhibitors of ebolavirus entry. Since these inhibitors will bind to the virus in the endosome, all biophysical analyses were performed at pH 5.8 to mimic endosomal pH.

To produce a smaller target that presents a 100% identical region of the N-trimer (across all ebolavirus species), IZ_m was fused to the N-terminal 21 amino acids of the N-trimer, resulting in eboIZN21 (Fig. 2). Circular dichroism indicates that eboIZN21 is highly helical [Fig. 3(B)], and AUC and gel filtration studies show that it is largely trimeric with a slight tendency to form higher order aggregates (Table I and Supporting Information Fig. S1). X-ray crystallography studies confirm the trimeric

Table I. *Biophysical Analyses of N-Trimer Mimics Via CD and AUC*

Peptide	$[\theta_{222\ nm}]$ (deg cm^2 dmol^{-1}) 25°C	$[\theta_{222\ nm}]$ (deg cm^2 dmol^{-1}) 37°C	$[\theta_{222\ nm}]$ (deg cm^2 dmol^{-1}) 50°C	M_{obs}/M_{calc} 4°C
eboIZN39IQ	−29,400	−27,900	−27,100	3.24
eboIZN39IQ(D3)	−30,400	−29,300	−28,400	3.22
eboIZN21	−25,500	−24,000	−22,900	3.54
eboIZN21(D2)	−24,800	−22,800	−21,800	3.15

CD scans were performed on the same samples of 11.4 μ*M* eboIZN39IQ, 11.1 μ*M* eboIZN39IQ(D3), 18.0 μ*M* eboIZN21 and 25.3 μ*M* eboIZN21(D2) in 50 m*M* sodium phosphate, pH 5.8, 150 m*M* NaCl at 25, 37, and 50°C. The peptides were allowed to equilibrate at each temperature for 10 min, after which no change in signal was seen over time. Sedimentation equilibrium analysis was performed on each peptide at three concentrations each (a starting concentration and two twofold dilutions, with typical starting concentrations between 10 and 30 μ*M*) and a minimum of two speeds, but typically three speeds (18,000, 21,000, and 24,000 rpm). Each data set was globally fit to a single ideal species. Each sedimentation equilibrium analysis was performed 2–4 times and averaged for the above table.

coiled-coil structure of eboIZN21 (below). As seen with eboIZN39IQ, eboIZN21 is very stable, showing similar CD spectra at 25, 37, and 50°C (Table I). We also attempted to produce mimics presenting the C-terminal portion of the N-trimer, but they were not soluble (data not shown) and were not studied further.

As negative controls for binding studies and drug discovery efforts, we produced mutant N-trimer mimics aimed at abolishing the C-peptide binding site. Specifically, alanines found along the C-peptide binding groove were mutated to aspartate, introducing binding-disruptive charges along the groove (Fig. 2). The resulting peptides are termed eboIZN39IQ(D3) and eboIZN21(D2). Using CD and AUC, we confirmed that these mutants maintained the stable coiled-coil structure and trimeric nature of their wild-type counterparts (Fig. 3 and Table I).

C-peptide binding characterization

To validate that eboIZN39IQ presents the native conformation of the N-trimer found in the prehairpin intermediate, we characterized binding to its native C-peptide ligand (Fig. 2), which binds along the entire groove of the N-trimer in the postfusion trimer-of-hairpins conformation. Surface plasmon resonance (SPR) analysis (ProteOn XPR36, Bio-Rad) of the interaction of the full-length C-peptide, eboC37, with eboIZN39IQ showed a dissociation constant of 14 n*M* (Fig. 4), with no binding to the D3 negative control. This tight binding affinity is of the same magnitude as the HIV-1 N-trimer/C-peptide interaction[29] and indicates that eboIZN39IQ presents a native N-trimer. A shortened C-peptide (eboC24), missing the 13 N-terminal residues of eboC37, bound to eboIZN39IQ with a dissociation constant of ~300 n*M* and did not bind to the D3 negative control (Supporting Information Fig. S2). eboIZN21 was less well behaved on an SPR surface, and we were unable to obtain reproducible data using this target.

Crystal structure of eboIZN21

To visualize how the N-trimer is presented in the absence of the native C-peptide ligand, as in our

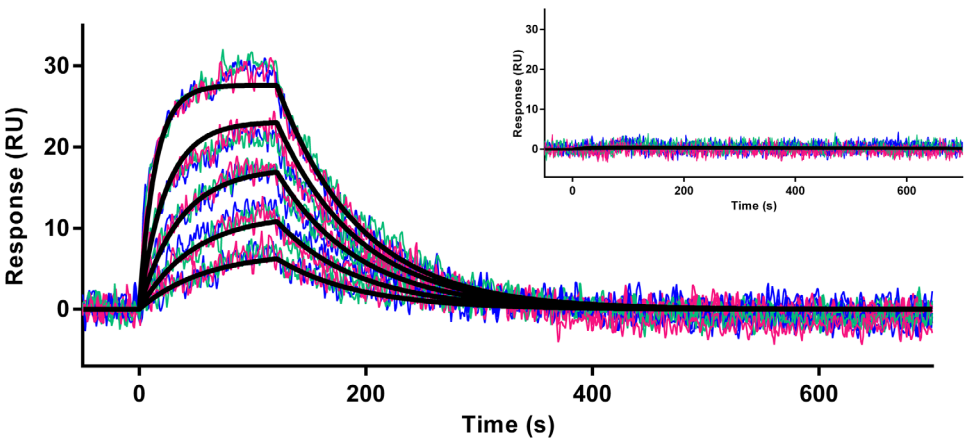

Figure 4. Binding of the ebolavirus C-peptide to the N-trimer mimic. Sensorgram of eboC37 flowed over eboIZN39IQ in a triplicate twofold dilution series starting at 60 n*M*, plotted with second-order second-neighbor-smoothing with a Savitzky–Golay filter (Prism 6, GraphPad Software). Each replicate dilution series is shown as a distinct color. The kinetic fit of the raw data is shown and yields $k_a = 9.6 \times 10^5\ M/s^1$, $k_d = 0.014/s^1$, and a K_D of 14 n*M*. Inset: The same eboC37 dilutions flowed over an eboIZN39IQ(D3) surface. No binding was observed.

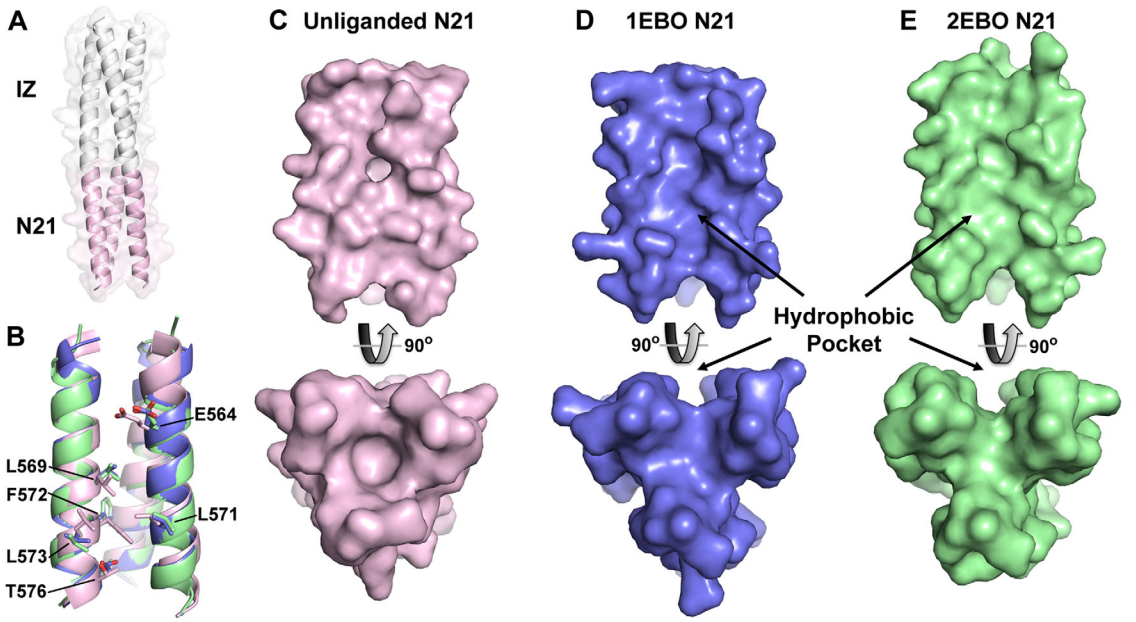

Figure 5. Crystal structure of eboIZN21. (A) Cartoon rendering with a semitransparent surface of the unliganded eboIZN21 structure. The IZ trimerization domain (white) and N21 region (pink) are indicated. The N21 region of available ebolavirus N-trimer structures is shown in isolation in panels B–E. (B) Overlay of the N21 region of the unliganded structure with the N21 region of the two previously solved ebolavirus GP2 core structures containing C-peptide (PDB IDs: 1EBO and 2EBO shown as blue and green, respectively. This color scheme is maintained in panels C–E). Residues that line the N21 groove and have significantly different rotamer conformations in the unliganded structure are shown as sticks and labeled. These residues occupy some of the equivalent space occupied by C-peptide (not shown) in the liganded structures resulting in a less prominent hydrophobic pocket when viewed (in subsequent panels) as a surface. (C) Surface representation of the unliganded N21 region. The bottom panel is the view of N21 from the bottom along its threefold axis and is rotated approximately 90° as compared to the top panel. (D, E) Similar views to (C) of the N21 region from the structures containing C-peptide. The prominent hydrophobic pocket in the 1EBO and 2EBO structures appears to be induced by ligand binding since the pocket is nearly absent in the unliganded structure.

mimics, we determined the X-ray crystal structure of eboIZN21 to 2.15 Å. eboIZN21 crystallized as a symmetrical trimer in space group P321 with one monomer in the asymmetric unit. The structure reveals that eboIZN21 is a continuous trimeric coiled coil, as designed [Fig. 5(A)]. Comparing our structure with the two previously reported structures of the ebolavirus 6-helix bundle (PDB IDs: 1EBO[28] and 2EBO[27]) revealed good overall agreement between the N21 residues of our unliganded structure and the C-peptide-bound structures, as indicated by root mean square deviations (rmsd) of 1.2 Å (across 63 atoms, 1EBO) and 1.4 Å (across 61 atoms, 2EBO) when trimers are aligned on Cα residues [Fig. 5(B)]. However, surface renderings show that a hydrophobic pocket in the N21 region of the 6-helix bundle structures, which accommodates residues 619–626 of the bound C-peptide, is collapsed in the isolated eboIZN21 structure [Fig. 5(C–E)].

The collapse of this pocket in the unliganded structure results from the side-chain conformations of several residues that fill the pocket. Specifically, in the absence of C-peptide, residues L569, L571, F572, L573, and T576 adopt alternate rotamers to pack together via hydrophobic interactions and thus alter the surface contours of the ligand binding pocket (Supporting Information Fig. S3). The side chain of E564 also adopts an alternate conformation to occupy a distinct portion of the pocket (toward the top of the pocket in Fig. 5). Therefore, as seen with the analogous hydrophobic ligand-binding pocket in the HIV gp41 N-trimer [comparing structures in Refs. (29–32), e.g., Supporting Information Fig. S4], our eboIZN21 unliganded structure indicates that the ebolavirus GP N21 pocket is induced by ligand binding and can likely adopt various conformations depending on the specific ligand.

We used the MONSTER protein interaction server[33] to calculate the solvent accessible surface area (SASA) buried at the interface of the ebolavirus and HIV hydrophobic pockets with their C-peptides. The crystal structures of the ebolavirus[27,28] and HIV[30,31] 6-helix bundles reveal that in each case the pocket interacts with 8 C-peptide residues (ITDKIDQI for ebolavirus and WMEWDREI for HIV) [Supporting Information Fig. S4(A,C)]. The buried SASA at the N21 pocket/8-mer C-peptide interface is similar in the 1EBO and 2EBO structures at 393/348 and 387/325 Å^2, respectively. These values are comparable to SASA buried at the HIV gp41 pocket/8-mer

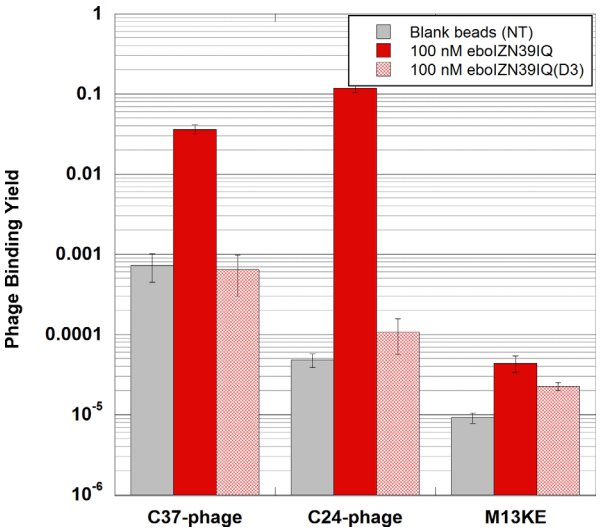

Figure 6. Validation of eboIZN39IQ as a phage display target. Clonal phage expressing ebolavirus C-peptides (eboC37 or eboC24) were incubated with biotinylated eboIZN39IQ in solution followed by capture via magnetic streptavidin beads. Negative target controls include the binding site mutant, eboIZN39IQ(D3), and magnetic beads with no target (NT). Binding of M13KE (phage with no peptide clone) to all targets was also assayed. The fraction of phage bound is reported. Error bars represent standard error across triplicate experiments.

C-peptide interface (349/310 Å^2).[30] Finally, a similar analysis between the HIV pocket and our D-peptide entry inhibitor, PIE12 [Supporting Information Fig. S4(B)], reveals that 416/391 A^2 of SASA is buried at that interface.[32] Given the comparable size of the pocket/C-peptide interface in the ebolavirus and HIV 6-helix bundle structures, combined with the high anti-HIV potency of PIE12-trimer (a trimerized version of PIE12, designed to bind all three pockets of the prehairpin intermediate),[32] it is reasonable to expect that potent pocket-specific peptide inhibitors of ebolavirus can also be discovered.

Phage display target validation

Phage display is a powerful screening technology that is used to screen billions of peptides or antibodies against a target of interest to identify specific inhibitors of protein/protein interactions. Indeed, HIV N-trimer mimics were successfully used in phage display screens of both scFv antibodies and D-peptides (see "Mirror-Image Phage Display" below) to identify potent, broadly neutralizing HIV entry inhibitors.[25,29,32,34,35] To validate the ebolavirus N-trimer mimics as discovery targets in the context of phage display, we produced phage clones expressing the native binding partners eboC37 and eboC24 [Fig. 2(A)] and assayed their ability to bind to our N-trimer mimics in phage clone binding assays. These experiments were designed to verify ligand binding and to define the best conditions for future phage display discovery efforts.

Phage display selections can be conducted in two formats: solid- and solution-phase. In solid-phase selections, the target is bound to a solid support (here, biotinylated ebolavirus N-trimer mimic is attached to streptavidin-coated magnetic beads), and then the phage are incubated with the immobilized target. Since common phage display libraries are multivalent (multiple copies of the library molecule are expressed on the surface of the phage, due to fusion to multicopy coat proteins), avidity effects improve the apparent binding constant of the library clones. This avidity-induced affinity boost is beneficial when screening naïve phage libraries, where initial binders typically have low target affinities. In solution phase, where both target and phage are incubated in solution, avidity effects are reduced. Following incubation, the bound complexes are captured through a brief interaction with a solid support (again, in this case, through a biotinylated target and streptavidin beads). At equivalent target concentrations, solution-phase selection is more stringent than solid-phase selection. The higher stringency of solution-phase is useful when screening second-generation libraries for affinity maturation (e.g., peptide binding consensus libraries or antibody variable loop mutagenesis libraries), where tight binders must be distinguished from a background of moderate binders.

Both eboC37 and eboC24 clonal phage bound to eboIZN39IQ target significantly over background (both empty beads and negative control eboIZN39IQ(D3) beads) using solution-phase clonal phage binding assays carried out at pH 5.8 to mimic the endosomal environment (Fig. 6). Also, binding of M13KE empty phage to both eboIZN39IQ and eboIZN39IQ(D3) was minimal. These data validate eboIZN39IQ as a phage display target. In addition, these data demonstrate that eboIZN39IQ(D3) serves as an effective negative control, as its clonal C-peptide phage binding is comparable to that of blank beads. In this format, both C-peptide clones bound at similar levels to eboIZN39IQ, although eboC37 had greater background binding to both negative controls.

Specific binding (over two orders of magnitude over background) was seen when using eboIZN21 as a target in a solid-phase eboC24 clonal phage binding assay, also validating eboIZN21 as a phage display target (Fig. 7). With the low level of eboC24 phage binding to eboIZN21(D2) (similar to eboC24 binding to blank beads), the binding site mutant is also verified as a negative control. In addition, only a very low level of M13KE empty phage binding to eboIZN21 and eboIZN21(D2) was observed.

Low phage background binding to targets is required in order to discern specific binding during

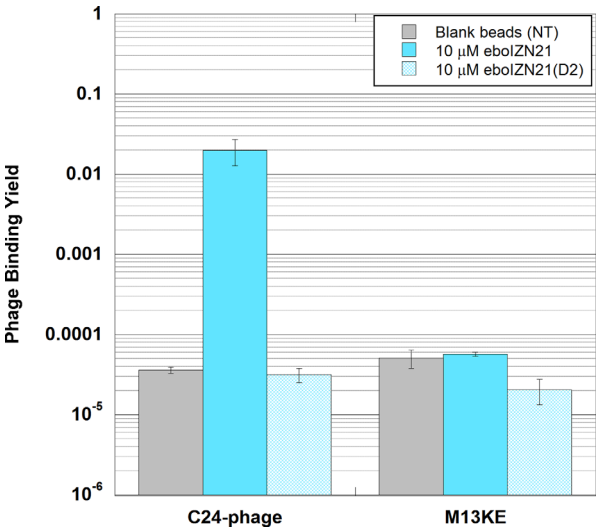

Figure 7. Validation of eboIZN21 as a phage display target. Clonal phage expressing an ebolavirus C-peptide (eboC24) were incubated with biotinylated eboIZN21 bound to streptavidin magnetic beads (solid-phase conditions). Negative target controls include the binding site mutant, eboIZN21(D2), and magnetic beads with no target (NT). Binding of M13KE (phage with no peptide clone) to all targets was also assayed. The fraction of phage bound is reported. Error bars represent standard error for triplicate experiments.

phage panning rounds. To evaluate this property for our two N-trimer mimics, we analyzed empty M13KE phage binding to both targets under varying conditions (Fig. 8). In both solid- and solution-phase formats, M13KE phage showed significantly higher binding to eboIZN39IQ beads than to blank beads. For the eboIZN21 target, phage background binding was drastically reduced in comparison to eboIZN39IQ, and binding of M13KE phage was similar to both target and blank beads in solid and solution phase. Under stringent conditions (solution phase, 100 n*M* target) the M13KE background binding to eboIZN39IQ was minimized, and a large affinity difference for eboC24 binding to eboIZN39IQ versus eboIZN21 could be seen. This affinity difference is likely to be biologically relevant because the trimer-of-hairpins structures[27,28] show that the binding site of eboC24 extends past the C-terminus of N21. These data indicate the importance of choosing proper stringency conditions in performing phage display selections.

The first step of a phage display discovery process is to screen a naïve phage display library for binding to the desired target. In such a first selection, where the library diversity only partially samples the large potential sequence space (e.g., a naïve peptide 12-mer library has 20^{12} ($>10^{15}$) possible sequences, whereas the typical diversity of a phage display library is $<10^{10}$), the best binders identified are usually modest, with low- to mid-micromolar affinities. Therefore, the selection pressure applied during phage panning must also be modest. Standard naïve phage display starting conditions are 10 μ*M* target presented on solid-phase (i.e., 30 μL of 10 μ*M* target immobilized onto magnetic beads).[25] As illustrated in Figure 8, M13KE binding to eboIZN39IQ is nearly saturated at this condition, and therefore it would not be possible to identify binding over background. 10% phage binding is considered saturating, as binding yields of even strong binders do not generally exceed this level (likely due to proteolysis of displayed peptides). Under the same conditions, the eboIZN21 background binding is >600-fold lower and similar to blank bead binding, ideal starting conditions for naïve phage display. Therefore, eboIZN21 is an optimized target for phage display discovery efforts. Additionally, the eboC24-phage can serve as an important positive control during naïve phage display to validate the conditions used to capture weak, but specific binders. Notably, in addition to having ideal behavior in phage display, the N21 region is also identical across all ebolavirus species and highly conserved among filoviruses (95% conserved) [Fig. 2(A)]. eboIZN39IQ is an ideal target for higher stringency solution-phase phage display and could be used to screen secondary libraries for affinity optimization of ligands identified from the naïve library. This could be especially useful for extending the binding interface of the ligands further along the N-trimer groove.

Mirror-image phage display

Mirror-image phage display is an innovative adaptation of standard peptide phage display and is used to identify D-peptides that bind to a target of interest[25,36] (Supporting Information Fig. S5). D-peptides are composed of D-amino acids and are the mirror-image of naturally occurring L-peptides. D-peptides have several important potential advantages as drug candidates (as reviewed[37]). As peptides, they are capable of blocking large protein/protein interactions, which is generally not possible for small molecules. In addition, because they are resistant to protease degradation,[38] D-peptides should possess a longer *in vivo* half life and reduced immunogenicity.[39] In our HIV-1 entry inhibitor discovery program,[18,25,29,32] we used mirror-image phage display and protein design to develop the highly potent and broadly acting D-peptide entry inhibitor, chol-PIE12-trimer, which is now in advanced preclinical studies. Their resistance to endosomal proteases makes D-peptides especially attractive as ebolavirus entry inhibitors. Our future studies will therefore use the N-trimer mimics to discover D-peptide inhibitors of ebolavirus entry by mirror-image phage display.

In traditional peptide phage display, a library of phage, each with a unique peptide displayed on its surface, is screened against a target.[40] In mirror-image phage display, the target is chemically

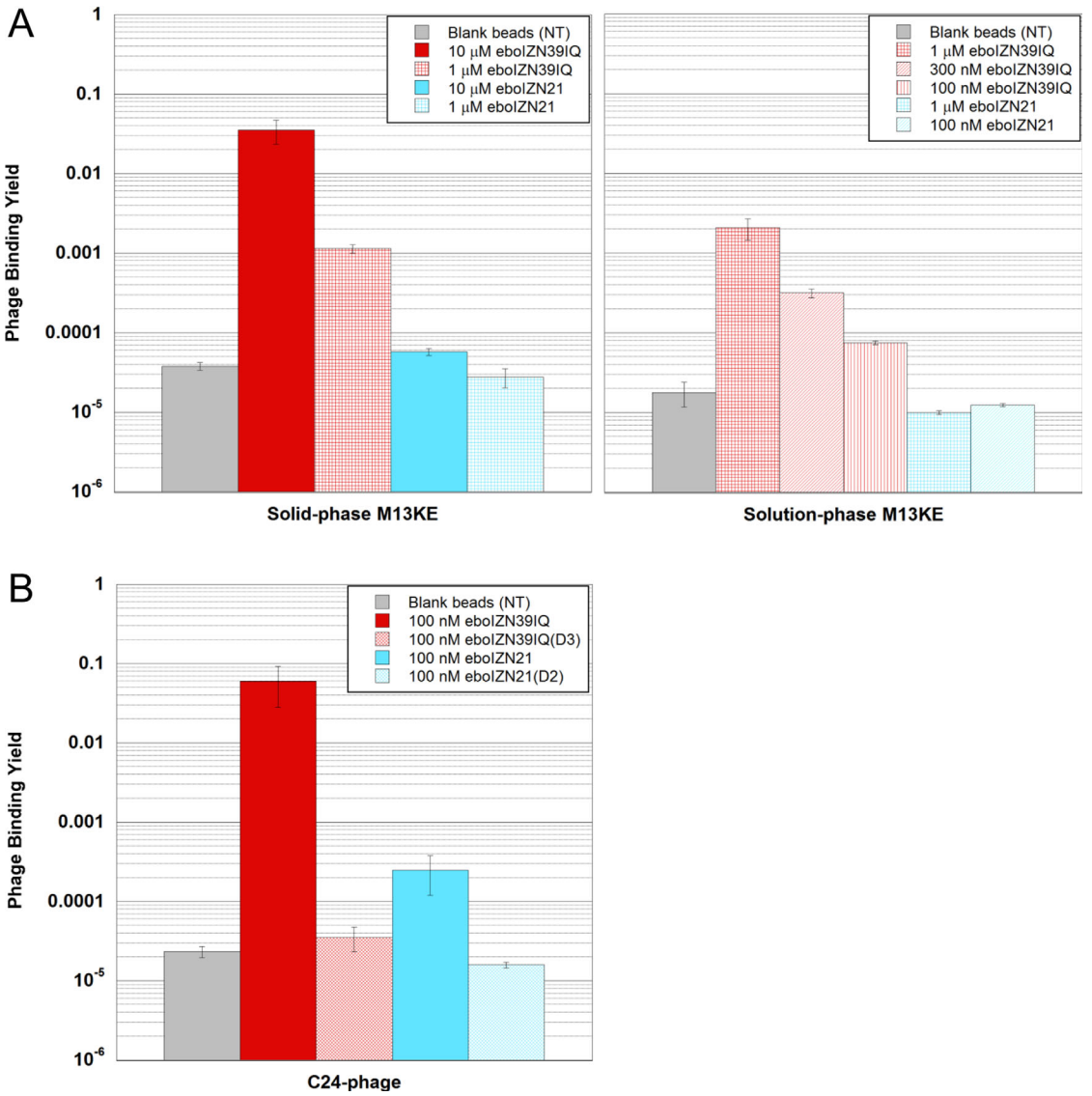

Figure 8. Comparing the two ebolavirus N-trimer mimics as phage display targets. (A) Phage background binding is greater to eboIZN39IQ than to eboIZN21. Phage binding assay showing M13KE control phage binding to biotinylated eboIZN39IQ and eboIZN21 under both solid-phase (left) and solution-phase (right) conditions. Magnetic beads with no target (NT) were used as a negative control. The fraction of phage bound is reported. Error bars represent the range for duplicate experiments (solid phase) and standard error for four or more replicates (solution phase). (B) High stringency solution-phase binding shows an affinity difference for the specific binding of eboC24 to the two N-trimer mimics. Clonal phage expressing eboC24 were incubated with biotinylated N-trimer in solution followed by capture via magnetic streptavidin beads. Negative target controls include the binding site mutants and magnetic beads with no target (NT). For NT, error bars represent standard error across triplicate experiments. The remaining error bars represent the range for duplicate experiments.

synthesized from D-amino acids and therefore forms the mirror-image structure of the natural L-target (Supporting Information Fig. S5). Phage display using the D-target is performed, and identified L-peptides that bind the D-target are then chemically synthesized using D-amino acids. By the law of symmetry, these D-peptides bind the natural L-target. Unlike with traditional phage display, mirror-image phage display targets are limited in size to those that can be chemically synthesized (although this size limit is continually expanding with modern chemical protein synthesis advances[41].

In order to prepare ebolavirus N-trimers as mirror-image phage display targets, we synthesized them as D-peptides. At 48 amino acids each, D-eboIZN21 and D-eboIZN21(D2) were synthesized through standard solid-phase peptide synthesis (SPPS) techniques. Importantly, even though the 101-residue length of eboIZN39IQ is beyond the scope of standard SPPS, modern chemoselective ligation techniques[42] allow for its assembly from multiple peptide segments. D-eboIZN39IQ, was assembled using native chemical ligation[43] and metal-free desulfurization,[44] in which cysteine residues are

introduced at native alanine sites to facilitate ligation and then converted back to alanine through desulfurization [Supporting Information Fig. S6(A)]. D-eboIZN39IQ was assembled from three synthetic segments of 27–41 residues. The production of D-eboIZN39IQ(D3) required a different assembly strategy, as one of the alanines used in D-eboIZN39IQ as a ligation junction is mutated to aspartate. Therefore, D-eboIZN39IQ(D3) was assembled from two synthetic segments of 33 and 68 amino acids. The final peptide products were confirmed by LC/MS [e.g., Supporting Information Fig. S6(B,C)].

The law of symmetry dictates that D-peptides will adopt the mirror-image structure of their L-counterparts. CD analysis of D-eboIZN21 confirms it possesses mirror-image helical structure compared to its L-peptide counterpart [Supporting Information Fig. S7(A)]. SPR analysis of D-eboC37 binding to D-eboIZN39IQ shows a similar binding affinity (6 n*M*) to the L-peptide interaction and validates the functionality of D-eboIZN39IQ [Supporting Information Fig. S7(B)]. Preliminary phage display experiments with these D-targets demonstrate the same M13KE binding properties as the L-versions (data not shown), verifying the strategy of screening naïve libraries with the D-eboIZN21 target and employing D-eboIZN39IQ for subsequent affinity optimization efforts when higher stringency is appropriate.

Vulnerability of the Ebolavirus prehairpin intermediate to a high potency inhibitor

A prerequisite for the success of drug discovery efforts targeting the ebolavirus N-trimer mimics is the exposure of a vulnerable prehairpin intermediate during viral entry. Exogenous C-peptides derived from the transmembrane subunit of the envelope glycoprotein have been used to validate this vulnerable prehairpin intermediate in a variety of viruses (e.g., HIV, SARS, and many paramyxoviruses[45–47]). For ebolavirus, an early report showed C-peptide inhibition activity at mM concentrations,[48] and more recent reports describe improved inhibitory activity (mid μM) of C-peptides with an endosomal localization tag.[49,50] Our ebolavirus N-trimer, eboIZN39IQ, provides an additional tool with which to explore the vulnerability of the prehairpin intermediate. In support of this strategy, peptide mimics of the HIV-1 N-trimer inhibit HIV entry at mid nM concentrations by binding to the C-peptide region of the exposed intermediate.[24]

Indeed, eboIZN39IQ inhibited entry in our pseudovirus system in which ebolavirus GP (representative species, *Zaire ebolavirus*) is expressed on the surface of an HIV particle [Fig. 9(A)], with an average IC_{50} of 320 n*M*. Importantly, the anti-ebolavirus activity of our negative control, eboIZN39IQ(D3), is ~30-fold diminished, with an IC_{50} of 11 μ*M*. It is difficult to determine the exact nature of the modest

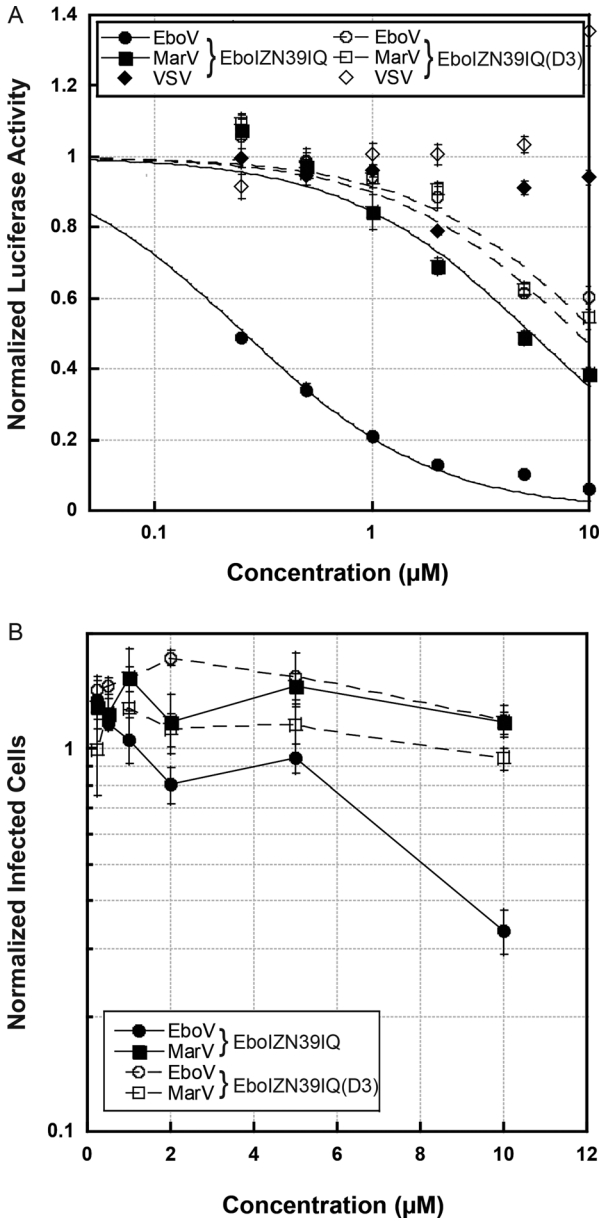

Figure 9. Inhibition of filovirus entry by eboIZN39IQ. (A) A representative pseudovirion assay looking at the inhibitory activity of eboIZN39IQ and the negative control, eboIZN39IQ(D3) against ebolavirus (EboV), marburgvirus (MarV), and VSV retroviral pseudotypes. Each point represents the average of quadruplicate measurements normalized to uninhibited control. Error bars represent normalized standard errors. For this particular assay, eboIZN39IQ IC_{50}s are 260 n*M* against ebolavirus and 5.4 μ*M* against marburgvirus. The eboIZN39IQ(D3) IC_{50}s are 8.9 μ*M* against ebolavirus and 11 μ*M* against marburgvirus. (B) Data for the authentic filovirus immunofluorescence inhibition assay. Each point represents the average of quadruplicate measurements normalized to vehicle control. Strong inhibition of ebolavirus is seen at 10 μ*M* eboIZN39IQ, with an average 33% (±4%) of infected cells compared to vehicle control.

eboIZN39IQ(D3) activity, as it is not seen against a vesicular stomatitis virus glycoprotein pseudotype (VSV), and no morphological changes (indicative of

toxicity) were observed. It is possible the modest eboIZN39IQ(D3) activity could be due to residual prehairpin intermediate binding activity. eboIZN39IQ demonstrated modest activity against marburgvirus pseudovirions (another member of the filovirus family), at an IC_{50} of 5.7 μM, although this was only ~2-fold better than the eboIZN39IQ(D3) anti-marburgvirus activity.

The ability of eboIZN39IQ to inhibit the entry of wild-type ebolavirus and marburgvirus was also assessed using a filovirus immunofluorescence assay under BSL4 conditions [Fig. 9(B)]. Although eboIZN39IQ was significantly less potent in this assay, there is 67% inhibition of entry at the highest concentration tested (10 μM) and no inhibition by our negative D3 control. Also, no activity was seen against marburgvirus. Potency differentials between pseudovirus systems and authentic filoviruses have been seen for other fusion inhibitors [for example in Ref. (51)]. Taken together, these data validate the presence of a vulnerable prehairpin intermediate during the ebolavirus entry process.

Unlike HIV-1, ebolavirus enters cells via endocytosis and initiates membrane fusion late in the endosomal pathway. Therefore, ebolavirus entry inhibitors will have to enter into and be active in endosomes. Although eboIZN39IQ does not possess a specific tag to localize it to endosomes, it is highly charged on its surface (with both positive and negatively charged side chains), and, interestingly, the inhibitory activity we observed in both the pseudovirus and authentic ebolavirus systems was dependent on the presence of the standard viral assay additive DEAE-dextran. It seems likely that the highly charged N-trimer mimic associates with the anionic cell membrane, especially in the presence of the cationic DEAE-dextran that would reduce electrostatic repulsion between the negative charges of eboIZN39IQ and the membrane, allowing it to access the endosome more efficiently than C-peptides.[50] As a structured peptide, eboIZN39IQ would also likely resist proteolysis longer than unstructured C-peptides.

Conclusion

In summary, we have designed and characterized two mimics of the highly conserved ebolavirus GP N-trimer region as it appears in the prehairpin intermediate during viral entry. In addition, through our clonal phage display experiments, we have functionally validated eboIZN39IQ and eboIZN21 as drug discovery targets, especially for phage display screens. Finally, with the characterization of the inhibitory activity of eboIZN39IQ, we have further validated the vulnerability of the ebolavirus prehairpin intermediate by demonstrating potent inhibition. These N-trimer mimics should be valuable for the discovery of small molecules, antibodies and/or peptides that inhibit ebolavirus entry. Specifically, our group is interested in the discovery of D-peptide inhibitors of ebolavirus using mirror-image phage display, and with the two targets and their binding site mutants synthesized in the D configuration, we are now poised for those selections.

It is noteworthy that in addition to the remarkable conservation of the N-trimer region across all ebolavirus species, it is also highly conserved across the filovirus family [see Fig. 2(A)]. Therefore, discovery efforts will likely identify inhibitors with broad filovirus activity. If such activity is suboptimal, it should be possible to design analogous mimics of the marburgvirus N-trimer region and use them in concert with the ebolavirus targets. For example in phage display, rounds of panning could alternate between the ebolavirus and marburgvirus targets, selecting specifically for an inhibitor of both viruses. Although the vast majority of natural filovirus outbreaks have been caused by ebolavirus, marburgvirus still poses a risk both as a natural pathogen (with three outbreaks in the last 10 years) and as a bioterror agent,[52] making the discovery of a broad-spectrum inhibitor desirable.

In addition to serving as drug targets, the ebolavirus N-trimer mimics should be useful as cell biological tools. For example, fluorescently labeled N-trimers could be used in cell culture experiments to track the appearance of the prehairpin intermediate during the viral entry event. Such studies would advance insight into filovirus entry dynamics.

Materials and Methods

Reagents

Plasmids and cells were obtained from the indicated sources: pEBB-HXB2 (gift from B. Chen)[53], SV-ZeboGPΔmuc and SVMarVGP (gift from M. Farzan),[54] BLR(DE3)pLysS *E. coli* (EMD Millipore, Billerica, MA), BL21-Gold(DE3)pLysS *E. coli* and XL-1 Blue *E. coli* (Agilent Technologies, Santa Clara, CA). pNL4–3.Luc.R-E- (N. Landau)[55,56] and HOS-CD4-fusin (N. Landau)[57,58] were obtained from the NIH AIDS Research and Reference Program. Mammalian cells were propagated in standard tissue culture medium, Dulbecco's Modified Eagle Medium (DMEM) supplemented with 10% fetal calf serum and L-glutamate (Life Technologies, Grand Island, NY).

Recombinant peptide production and purification

The DNA encoding eboIZN39IQ and eboIZN39IQ(D3) was produced via PCR gene synthesis. The IZ_m and IQ fragments were PCR amplified from plasmids encoding HIV-1 N-trimer mimics [e.g. in Ref. (59)]. An *Nde*I site was included in the 5′ PCR primer for IZ_m, and a *Bam*HI site was included in

the 3′ PCR primer for IQ. The ebolavirus N39 sequence from the species *Zaire ebolavirus*[60] was synthesized in two overlapping oligos with optimized codons and companion primers. All internal primers contained complementary sequences so the three separate components, IZ_m, N39, and IQ could be annealed and amplified together. The resulting DNA fragment was cloned into the *Nde*I/*Bam*HI cloning sites of pKA8, validated by sequencing and expressed in BLR(DE3)pLysS cells using an autoinduction protocol. Specifically, cultures were inoculated from a single colony and grown overnight at 37°C in autoinduction media.[61] The resultant peptide has an N-terminal His tag (His_8) followed by a TEV cleavage site (ENLYFQG). A single tyrosine was placed at the end of the sequence to facilitate concentration determination via absorbance at 280 nm. The peptides were resuspended from inclusion bodies using Ni-binding buffer (20 n*M* sodium phosphate pH 8.0, 300 m*M* NaCl, 10 m*M* imidazole) + 6*M* GuHCl, and purified via gravity flow Ni affinity chromatography (HIS-Select Nickel Affinity Gel, Sigma Aldrich, St. Louis, MO). The purified peptides were dialyzed into 5% acetic acid and further purified by reverse phase HPLC on a C18 column (Vydac, Grace, Columbia, MD) and lyophilized. Peptide powder was resuspended in water and diluted to 0.2 mg/mL in 50 m*M* sodium phosphate pH 6.5, 0.5 m*M* EDTA, 1 m*M* DTT and digested with a solubility-enhanced tobacco etch virus NIa protease (TEVse, based on published modifications[62,63]) overnight at 30°C. The digested peptide was dialyzed into 5% acetic acid and then HPLC purified and lyophilized. The final peptide sequences are: GHMD**IKKEIEAIKKEQEAIKKKIEAIEKE***LRQLAN ETTQ(A/D)LQLFLR(A/D)TTELRTFSILNRK(A/D)ID FLLQR***MKQIEDKIEEIESKQKKIENEIARIKKLIG ER**Y**, with IZ_m and IQ shown in bold, the ebolavirus N-trimer in italics, and the three alanine positions that are changed to aspartate in the D3 mutant in parentheses.

Biotinylated eboIZN39IQ and eboIZN39IQ(D3) for SPR analysis and phage display were expressed from plasmids that are modified from those described above. Using PCR, a CGG sequence was added N-terminal to IZ (GHMCGGDIKK…). Expression and purification were as described above with additional reduction steps included to keep the cysteine reduced during purification (100 m*M* DTT treatment after Ni++ affinity chromatography and 50 m*M* TCEP treatment after TEV digestion). The purified protein was biotinylated with EZ-link Maleimide–PEG2–biotin (Thermo Scientific, Waltham, MA). The purified lyophilized powder was resuspended at 1 m*M* in freshly prepared reaction buffer (6 *M* GuHCl, 150 m*M* NaCl, 100 m*M* Na_2HPO_4, 5 m*M* TCEP) and the biotinylation reagent was added at 5 m*M* and allowed to react for 4 h at RT. The biotinylated peptides were purified by reverse phase HPLC on a C18 column (Waters) and lyophilized. The mass of the peptide was confirmed by LC/MS (AB Sciex API 3000 LC/MS/MS system, Framingham, MA).

Peptide synthesis

eboIZN21, eboIZN21(D2), eboC37 and eboC24 were chemically synthesized using solid-phase peptide synthesis (SPPS) with Fmoc-amino acids (AAPPTec, Louisville, KY, and CBL Biopharma, Boulder, CO) on a Prelude peptide synthesizer [Protein Technologies (PTI), Tucson, AZ]. A single tyrosine was placed at the N-terminus of both eboIZN21 and eboIZN21(D2) to facilitate concentration determination via absorbance at 280 nm. The peptides were synthesized on TentaGel R RAM resin (Rapp Polymere, Germany) to yield C-terminal amide peptides. Standard synthesis scales were 25–32 μmol per peptide. Standard amino acid coupling was as follows: 3 × 3 min deprotection with 20% piperidine in DMF followed by 25 min couplings with 72.2 m*M* amino acid (200 m*M* stocks in NMP), 71.5 m*M* HATU (198 m*M* stock in DMF), and 166.7 m*M* NMM (600 m*M* stock in DMF). Biotinylation was achieved with N-Biotinyl-NH-$(PEG)_2$-COOH DIPEA (Novabiochem, EMD Millipore) coupling for 2 h. N-terminal capping was accomplished in 30 min with 2 mL acetic anhydride and 2 mL 0.6*M* NMM. Peptide cleavage from resin was accomplished offline with 92.5% TFA, 2.5% EDT, 2.5% TIS, 2.5% H_2O when the peptide contained Met or Cys residue(s) or with 95% TFA, 2.5% TIS, 2.5% H_2O in the absence of any Met/Cys residues followed by precipitation/washing with diethylether. All peptides were purified by reverse-phase HPLC on a Waters (Milford, MA) BEH X-Bridge C18 column (10 μm, 300 Å, 19 × 250 mm) with a water/ACN gradient in 0.1% TFA. All peptides were lyophilized and their molecular weight verified by LC/MS.

D-eboIZN39IQ was assembled from three synthetic peptide segments via native chemical ligation/metal-free desulfurization (Supporting Information Fig. S6). D-peptides were synthesized via Fmoc-SPPS on a PTI PS3 peptide synthesizer at 100 μmol scale. The C-terminal peptide was synthesized on Rink Amide AM resin LL (Novabiochem) and the other two segments were synthesized on Dawson Dbz AM resin (Novabiochem). The C-terminal segment contained an N-terminal cysteine residue in the place of a native alanine for use in native chemical ligation (CIDFLLQRMKQIEDKIEEIESKQKKIENEIARIKKLIGERY). For the same reason, the middle segment contained an N-terminal Boc-L-thiazolidine-4-carboxylic acid (Boc-Thz-OH, Bachem, Torrance, CA) as its N-terminal residue in place of the native alanine at that position((Thz)-NETTQALQLFLRATTELRTFSILNRK). The N-terminus of

the N-terminal peptide (GHMDIKKEIEAIKKEQEAIKKKIEAIEKELRQL) was biotinylated with N-Biotinyl-NH-(PEG)2-COOH DIPEA (Novabiochem). For peptides synthesized on Dawson Dbz AM resin, the C-terminal linker was converted to the resin bound *N*-acyl-benzimidazolinone (Nbz) according to manufacturer instructions. Cleavage of all peptides was performed according to standard procedures. Peptides were purified by reverse-phase HPLC on a Waters BEH X-Bridge C18 column (10 μm, 300 Å, 19 × 250 mm) with a water/acetonitrile gradient in 0.1% TFA. Ligations were performed according to Ref. (64) with peptide concentrations ~2 m*M*. Following ligation between the C-terminal and middle segments, the N-terminal Thz was converted to cysteine by dissolving the purified ligation product in 6*M* GuHCl, 200 m*M* sodium phosphate, 200 m*M* methoxyamine HCl, pH 4. After Thz to Cys conversion was achieved, the buffer was brought to 200 m*M* MPAA and 20 m*M* TCEP, the pH was adjusted to 7, and the N-terminal peptide was added to the solution for the final ligation. Following purification of the ligation product by reverse-phase HPLC, the cysteine residues at the ligation junctions were converted to the native alanine residues via a metal-free, radical-mediated desulfurization strategy essentially as described in Ref. (44) except that *t*-butylthiol was replaced with glutathione, and desulfurizations were performed at 37°C. eboIZN39IQ(D3) was synthesized in an analogous (though simplified) manner using two peptide segments.

Preparation of peptide samples for biophysical analysis

For biophysical analyses, peptide stocks were prepared in water from lyophilized peptide at concentrations of 400 μ*M* or greater for a minimum absorbance at 280 nm of 0.1 in a 1 cm pathlength cuvette. Stocks were centrifuged at 18,000*g* for 10 min to remove aggregates. Absorbance at 280 nm (using ϵ_{280} of 1408 M/cm^1 for tyrosine) was used to determine stock concentrations.[65] For eboIZN39IQ and eboIZN39IQ(D3), both recombinant and synthetic, UV absorbance consistently overestimated the concentration of the stocks (as evidenced by an unusually high 260/280 ratio as well as CD traces whose shape depicted ideal coiled coils but whose signal had a lower than expected absolute value). This overestimation is likely due to peptide bond absorbance contributing to the signal at 280 nm (101 amino acids with only one near-UV absorbing residue, a tyrosine). Therefore, the concentrations of these stocks were determined via quantitative amino acid analysis, which was performed using a Hitachi L-8800 Amino Acid Analyzer (Hitachi High-Technologies Corporation, Tokyo, Japan). Peptides were hydrolyzed in 5.7*N* HCl overnight at 105°C in sealed ampoules, and then analyzed via ion-exchange chromatography and postcolumn derivatization with ninhydrin using the Hitachi Analyzer. The peptides were then diluted to the desired concentration in 50 m*M* sodium phosphate pH 5.8, 150 m*M* NaCl. For eboIZN21 and eboIZN21(D2), all experiments described in this paper were performed with biotinylated peptide. For eboIZN39IQ and eboIZN39IQ(D3), CD, AUC and viral infectivity were performed with nonbiotinylated material, whereas SPR and phage display used biotinylated material.

Circular dichrosim

Circular dichroism (CD) data were obtained using an AVIV Model 410 spectrophotometer (AVIV, Lakewood, NJ). Samples were analyzed in a 1 mm pathlength quartz cuvette at 25, 37, and 50°C. Prior to CD analysis, prepared samples (in 50 m*M* sodium phosphate pH 5.8, 150 m*M* NaCl) were centrifuged at 18,000*g* for 10 min to remove aggregates. CD data were scanned in triplicate and buffer subtracted. Final CD data were presented according to mean residue ellipticity equation $[\theta] = 100 \times \theta/[(n - 1) \times (\ell) \times (c)]$, where θ is the observed ellipticity, $n - 1$ is the number of peptide bonds, ℓ is the pathlength in cm, and c is the peptide concentration in mM. Percent helicity was calculated from the ellipticity at 222 nm according to the Lifson–Roig-based helix-coil model which defines the dependence on chain length and temperature as described.[66] Due to aggregation observed with eboIZN39IQ and eboIZN39IQ(D3) upon initial dilution in the CD buffer, their final concentrations were corrected from the original amino acid analysis values based on the ratio of ellipticity at 222 nm post- and precentrifugation ($\theta_{222\text{-postspun}}/\theta_{222\text{-prespun}}$).

Analytical ultracentrifugation sedimentation equilibrium

Using an Optima XL-A Analytical Ultracentrifuge (Beckman Coulter, Brea, CA), sedimentation equilibrium analysis was performed on each peptide at three concentrations (a starting concentration and two 2-fold dilutions, with typical starting concentrations between 10 and 30 μ*M*). Dilutions were prepared in matching buffer (50 m*M* sodium phosphate, 150 m*M* NaCl, pH 5.8), and the same buffer was used for blanks. Each sample was spun until equilibrium, typically ~24 h, at a minimum of two speeds, but typically three speeds (18,000, 21,000 and 24,000 rpm). Each data set was globally fit to a floating molecular weight single ideal species with a nonlinear least squares algorithm as implemented in HETEROANALYSIS.[67] Fits are reported as the observed (i.e., fit) molecular weight divided by the calculated molecular weight of a monomer (M_{obs}/M_{calc}). Buffer densities and protein partial specific volumes were calculated with SEDNTERP (version

1.09).[68] For the biotinylated peptides, partial specific volumes were adjusted based on reported values for PEG.[69]

Surface plasmon resonance

SPR analysis was conducted on the Bio-Rad (Hercules, CA) ProteOn XPR36 instrument in PBS* running buffer (50 m*M* sodium phosphate, 150 m*M* NaCl, pH 5.8) + 0.1 mg/mL BSA and 0.01% Tween 20. Approximately 600 RUs of biotin-eboIZN39IQ (in the presence of eboC37) and biotin-eboIZN39IQ(D3) targets (200 n*M* stocks ultracentrifuged for 30 min at 45,000 rpm) were loaded at 67 n*M* on to the NLC neutravidin-coated chip (Bio-Rad), followed by blocking with 450 μ*M* biotin. Using the one-shot kinetics method, a twofold dilution series was performed in triplicate at RT starting at 60 n*M* for eboC37 and a threefold dilution series in triplicate at RT starting at 800 n*M* for eboC24. 10 min dissociation time for eboC37 and 5 min dissociation time for eboC24 were used to ensure the response fully recovered to baseline prior to the next injection. Data were corrected by subtracting blank surface and blank buffer reference injections, and the kinetics (for eboC37) and equilibrium (for eboC24) were globally fit to the Langmuir model for 1:1 binding[70] using ProteOn Manager software (Bio-Rad).

Crystallization

eboIZN21 was dissolved in ddH20 to a concentration of ~10 mg/mL and centrifuged at 18,000*g* for 10 min. Sitting-drop vapor-diffusion crystal trials were set up using a Phoenix crystallization robot (Art Robbins Instruments, Sunnyvale, CA). Crystals grew at 4°C in drops containing a 2:1 ratio of peptide to well solution, which consisted of 30% (v/v) 1,2-propanediol, 100 m*M* HEPES pH 7.5, 20% (v/v) PEG-400. The crystals were flash frozen in liquid nitrogen without the need for additional cryoprotection and determined to be in space group P321 with unit cell dimensions $a = b = 38.51$ Å, $c = 72.59$ Å.

Data collection, structure determination, and refinement

A native dataset was collected at beam line 7-1 of the Stanford Synchrotron Radiation Lightsource. Data were integrated and scaled to 2.15 Å resolution using HKL2000.[71] In order to rule out the possibility of twinning, data were initially scaled in space group P3 and analyzed with the program Xtriage,[71] which indicated that the data are untwinned and that the correct space group is P321. A model that consisted of a canonical helix appropriate to the size and sequence of the IZ domain and the N21 region of ebolavirus GP (PDB ID: 1EBO) was used for molecular replacement using the program Phaser.[72] A single eboIZN21 monomer was found in the asymmetric unit with the trimeric structure generated by the crystallographic threefold. Subsequent model building, structure refinement, and validation were performed with Coot,[73] PHENIX Refine,[74] and MolProbity[75] software, respectively. The final model was refined to crystallographic R/R_{free} values of 0.272/0.294 with good geometry (Supporting Information Table S1). Additional refinements were carried out in space group P3 allowing all possible twin laws, to further verify (by monitoring Rfree) that the correct space group is P321 with a monomer in the asymmetric unit. A composite omit map agreed well with the final model, indicating good sidechain density throughout. The atomic coordinates and structure factors have been deposited in the Protein Data Bank, http://www.pdb.org (PDB ID: 4R0R).

Clonal phage production

Forward and reverse sandwich oligonucleotides encoding the C-peptide clones were designed based on the primary sequence of each clone. The forward and reverse eboC37 oligonucleotides were: ATGCGG TACCTTTCTATTCTCATTCTTGGGGCGGCACCTGC CATATTCTGGGCCCGGATTGCGCGATTGAACCGC ATGATTGGACCAAAA and CCTTTTCGGCCGAACC CCCACCTTTATCCACAAAATCATGAATAATCTGAT CAATTTTATCGGTAATGTTTTTGGTCCAATCATGC GGTT. The forward and reverse eboC24 oligonucleotides were: ATGCGGTACCTTTCTATTCTCATTCT ATTGAACCGCATGATTGGACCAAAAACATTACCG and CCTTTTCGGCCGAACCCCCACCTTTATCCAC AAAATCATGAATAATCTGATCAATTTTATCGGTAA TGTTTTTGGTCCAATCATGCGGTT. The oligonucleotide sandwich was annealed with 5 μg of each primer in 50 μL total volume in ddH_2O by heating to 95°C and slow cooling and then extended with Klenow Fragment [New England Biolabs (NEB), Ipswich, MA] according to the manufacturer's protocol. The inserts and M13KE cloning vector backbone (NEB) were digested with Acc65I and EagI-HF. The insert DNA was EtOH precipitated, gel purified from a 6% TBE acrylamide gel, extracted from the gel by incubating gel slices in a minimal volume of extraction buffer (100 m*M* NaOAc pH 4.5, 1 m*M* EDTA, 0.1% SDS) for 16 h at 37°C, and ethanol precipitated. The inserts and plasmid backbone were ligated and transformed into SS320 electrocompetent cells and plated on LB/IPTG/X-gal plates (LB agar, 25 μg/mL tetracycline, 1 m*M* IPTG, 0.1 mg/mL X-gal). The DNA from specific phage plaques was PCR amplified and Sanger sequenced (Eton Bioscience, Durham, NC), and those containing the correct DNA were subsequently amplified from a single plaque.

Phage amplification

A single plaque was added to XL-1 Blue cells (OD_{600} 0.5–1), diluted to 40 mL of OD_{600} 0.05 in LB +25 μg/mL tetracycline, and shaken at 220 rpm at 37°C for

4.5–5 h. Cells were pelleted by centrifugation, and the phage supernatant was sterile filtered. Phage were precipitated by adding 1/6th volume of PEG-NaCl [20% w/v polyethylene glycol-8000 (Fisher Scientific, Pittsburgh, PA), 2.5*M* NaCl] and incubating overnight at 4°C. Precipitated phage were then pelleted via centrifugation and resuspended in TBS (50 m*M* Tris–HCl, 150 m*M* NaCl, pH 7.4). They were PEG-precipitated again (~1 h on ice), centrifuged and resuspended in 200 μL TBS. Aliquots were flash frozen and stored at −20°C with a working stock left at 4°C if imminent experiments were planned.

Clonal phage binding assay

For each phage binding reaction, 30 μL streptavidin-coated magnetic beads (Life Technologies, Dynabeads MyOne, Streptavidin T1) at 10 mg/mL were magnetically pelleted and washed with 3.3× bead volume TBS. The beads were then blocked in 3.3× bead volume 100% SB (Thermo Scientific, SuperBlock Blocking Buffer in TBS, pH 7.4) for 10 min at RT and rinsed with equal volume of 100% SB* (SB adjusted to pH 5.8 with HCl). Solution-phase beads were then resuspended in 3.3× bead volume of 100% SB* and stored at 4°C for up to 24 h. Solid-phase beads were resuspended in 3.3× bead volume PBS* + 10% SB*. To load target on to solid-phase beads, 1× bead volume of an appropriate target concentration (e.g., 10 μL of 10 μ*M* target for 10 μL beads) was added and incubated for 10 min followed by addition of 3.3× bead volume 5 m*M* D-Biotin (in PBS* + 10% SB*) and incubation for an additional 5 min. For blank (no target) beads, 3.3× bead volume of 5 m*M* D-Biotin was added and incubated for 5 min. All beads were then magnetically pelleted, washed in PBS*, and resuspended in 1× bead volume PBS* + 10% SB*.

Solid-phase binding reactions were incubated in 96-well format (Costar, sterile polystyrene, V-bottom, nontreated, Corning, Corning, NY) with shaking at 700 rpm for 2 h at RT either as 30 or 100 μL reactions in 1× PBST* (PBS* + 0.01% Tween 20) + 10% SB* and 10^{10} plaque-forming units (pfu) of the phage clone. All washes and elution were done on the KingFisher Duo magnetic particle processor (Thermo Scientific). The binding reaction was mixed on the KingFisher for 1 min at medium speed and the beads collected by 5 s dips of the magnet through the sample, repeated five times (5 × 5 s). All washes were done with PBST* (wash 1: 700 μL; wash 2: 800 μL; wash 3: 900 μL; washes 4–7: 1000 μL), mixed at slow speed for 1.5 min, and beads collected 3 × 3 s. Bound phage were eluted with 50 μL EB (0.2 *M* glycine, pH 2.2) for 10 min, beads collected 5 × 5 s, and neutralized with 7.5 μL NB (1 *M* Tris, pH 9.1). Dilutions of eluted phage were used to infect XL-1 Blue cells and then plated in top agar (40% LB agar/60% LB) on LB/IPTG/X-gal plates. Blue plaques were then counted to determine phage titers.

Solution-phase binding reactions were performed similarly to solid-phase 30 μL reactions. Instead of adding target-loaded beads to the binding reaction, an appropriate volume of 10× soluble target was added to the reaction (final 1× soluble target) just before phage were added. Additionally, on the Kingfisher Duo, target and bound phage were pulled down in a rapid 1 min magnetic pelleting step (1 min slow mixing, 5 × 5 s bead collect). All washes were done with PBST* except wash 1 which contained 5 m*M* D-Biotin to block unoccupied streptavidin sites (wash 1: 150 μL; wash 2: 700 μL; wash 3: 800 μL; wash 4: 900 μL; wash 5: 1000 μL), mixed at slow speed for 25 s, and beads collected 3 × 3 s.

Pseudovirus infectivity assays

Single-cycle pseudovirions were produced with a pNL4-3 HIV-1 genome (with firefly luciferase inserted into the nef gene and frameshift mutations in both Env and Vpr) and filovirus GP on their surface (or VSV for a specificity control). These pseudovirions were produced by co-transfecting 293T human embryonic kidney cells with the described HIV-1 genome (pNL4-3.Luc.R-E-) and a plasmid encoding the desired virus glycoprotein (SV-ZeboGPΔmuc for *Zaire ebolavirus* GP lacking the mucin domain, SV-MarVGP for marburgvirus (Musoke strain) GP and pMDG VSV-G for VSV) in the presence of polyethylenimine (PEI) transfection reagent (Polysciences, Inc., Warrington, PA). Pseudovirus-containing supernatant was collected and filtered through a 0.45 μ*M* filter 38–43 h post-transfection. For ebolavirus and marburgvirus, pseudovirions were concentrated by centrifuging through a 20% sucrose/TNE (10 m*M* Tris pH 7.6, 100 m*M* NaCl, 1 m*M* EDTA) cushion (26,000 rpm, 2 h), and the pellet resuspended in TNE, aliquoted and stored at −80°C.

To measure inhibition of infectivity, 90 μL of each inhibitor dilution and 8.9 μg/mL DEAE–dextran were added to HOS–CD4–fusion cells in a 96-well format. For each assay, a total of six inhibitor dilutions were tested, each in quadruplicate. The plates were transferred to BSL3, and 10 μL of pseudovirus diluted in media was added to each well 30–60 min after the inhibitor addition (final DEAE–dextran concentration of 8 μg/mL). Virus was diluted in order to yield a robust luciferase signal. 24 h later, all wells were inspected under a light microscope to check for gross morphological changes. Virus and inhibitor were removed via aspiration, and fresh media was replenished. 20–24 h later, the cells were lysed, and the luciferase activity was measured (Bright-Glo luciferase assay system, Promega, Madison, WI). To determine IC_{50} values, the data from each inhibitor concentration series were normalized

to the noninhibitor control signal and fit to a Langmuir equation: $y = 1/(1+[\text{inhibitor}]/IC_{50})$ (Kaleidagraph, Synergy Software, Reading, PA). The curve fit was weighted by the normalized standard error of each concentration point (with a minimum error allowed of 1%). Provided IC_{50}s are averages of two to four replicate experiments.

Filovirus immunofluorescence assays

Vero cells were seeded in 96 well black plates. Peptides and vehicle control were diluted to 1.1X final concentration in culture media [MEM, 5% FBS, gentamicin (10 μg/mL)] and 90 μL/well were incubated on the plate for 1 h at 37°C. In the BSL4 10 μL of virus diluted in media and DEAE–dextran was added to each well (final 8 μg/mL DEAE–dextran). Ebola virus (Kikwit, a representative strain of the *Zaire ebolavirus* species) and Marburg virus (Ci67) were diluted in culture media to yield a robust signal in the assay (∼20% infected cells). After 1 h at 37°C, the virus and peptides were removed, the wells were washed with PBS and media with peptide was used to replenish the wells. At 24 h postinfection, each well was visualized via light microscope to look for any gross morphological abnormalities. At 48 h postinfection, the wells were washed with PBS and then the cells fixed with 10% formalin. After blocking, the fixed cells were incubated with GP-specific mAb (9G4 for Marburg virus, KZ52 for Ebola virus) followed by incubation with FITC-labeled secondary antibody (goat antimouse or antihuman, respectively). Nuclei were stained with Hoechst solution. Cells were imaged using an Operetta high content device (PerkinElmer, Waltham, MA) and images were analyzed using Harmony software to determine percent of infected cells in a given well. Data were plotted normalized to the vehicle control.

ACKNOWLEDGMENTS

We thank Hyung Kim and Dennis Winge for amino acid analysis. We also thank Yu-Chan Chen, Andrew Steiner, Ruei-Lin Hsu, and Niladri Sinha for help with molecular biology, protein purification, and preliminary characterization of the N-trimer mimics and C-peptides. For help with peptide synthesis and purification, we thank Maritza Quintero and Dasha Pruss, and we thank Matthew Movsesian for assistance and advice. This research was funded by a University of Utah Funding Incentive Seed grant to D.M.E. and M.S.K., NIH grant AI102347 to B.D.W. and M.S.K, and NIH grant GM82545 to D.M.E. and C.P.H.. We thank the U.S. Air Force for support of T.R.C.. Portions of this research were carried out at the Stanford Synchrotron Radiation Light Source, (SSRL), which is supported by the U.S. Department of Energy, Office of Science, Office of Basic Energy Sciences. The SSRL Structural Molecular Biology Program is supported by the DOE Office of Biological and Environmental Research, and by the NIH, NIGMS. Opinions, conclusions, interpretations, and recommendations are those of the authors and are not necessarily endorsed by the U.S. Army, U.S. Air Force, the NIH or NIGMS. The mention of trade names or commercial products does not constitute endorsement or recommendation for use by the Department of the Army, the Department of Defense, or the U.S. Air Force.

REFERENCES

1. Sanchez A, Kahn AS, Zaki SR, Nabel GJ, Ksiazek TG, Peters CJ (2001) Fields virology. Philadelphia: Lippincott, Williams and Wilkins.
2. Centers for Disease Control and Prevention (2014) Chronology of Ebola hemorrhagic fever outbreaks. http://www.cdc.gov/vhf/ebola/resources/outbreak-table.html.
3. Baize S, Pannetier D, Oestereich L, Rieger T, Koivogui L, Magassouba N, Soropogui B, Sow MS, Keita S, De Clerck H, Tiffany A, Dominguez G, Loua M, Traore A, Kolie M, Malano ER, Heleze E, Bocquin A, Mely S, Raoul H, Caro V, Cadar D, Gabriel M, Pahlmann M, Tappe D, Schmidt-Chanasit J, Impouma B, Diallo AK, Formenty P, Van Herp M, Gunther S (2014) Emergence of Zaire Ebola virus disease in Guinea—Preliminary report. New Engl J Med 371:1418–1425.
4. Bossi P, Garin D, Guihot A, Gay F, Crance JM, Debord T, Autran B, Bricaire F (2006) Bioterrorism: Management of major biological agents. Cell Mol Life Sci 63: 2196–2212.
5. White JM, Delos SE, Brecher M, Schornberg K (2008) Structures and mechanisms of viral membrane fusion proteins: Multiple variations on a common theme. Crit Rev Biochem Mol Biol 43:189–219.
6. Volchkov VE, Feldmann H, Volchkova VA, Klenk HD (1998) Processing of the Ebola virus glycoprotein by the proprotein convertase furin. Proc Natl Acad Sci USA 95:5762–5767.
7. Volchkov VE, Volchkova VA, Stroher U, Becker S, Dolnik O, Cieplik M, Garten W, Klenk HD, Feldmann H (2000) Proteolytic processing of Marburg virus glycoprotein. Virology 268:1–6.
8. Carette JE, Raaben M, Wong AC, Herbert AS, Obernosterer G, Mulherkar N, Kuehne AI, Kranzusch PJ, Griffin AM, Ruthel G, Dal Cin P, Dye JM, Whelan SP, Chandran K, Brummelkamp TR (2011) Ebola virus entry requires the cholesterol transporter Niemann–Pick C1. Nature 477:340–343.
9. Chandran K, Sullivan NJ, Felbor U, Whelan SP, Cunningham JM (2005) Endosomal proteolysis of the Ebola virus glycoprotein is necessary for infection. Science 308:1643–1645.
10. Cote M, Misasi J, Ren T, Bruchez A, Lee K, Filone CM, Hensley L, Li Q, Ory D, Chandran K, Cunningham J (2011) Small molecule inhibitors reveal Niemann–Pick C1 is essential for Ebola virus infection. Nature 477: 344–348.
11. Misasi J, Chandran K, Yang JY, Considine B, Filone CM, Cote M, Sullivan N, Fabozzi G, Hensley L, Cunningham J (2012) Filoviruses require endosomal cysteine proteases for entry but exhibit distinct protease preferences. J Virol 86:3284–3292.
12. Schornberg K, Matsuyama S, Kabsch K, Delos S, Bouton A, White J (2006) Role of endosomal cathepsins

in entry mediated by the Ebola virus glycoprotein. J Virol 80:4174–4178.
13. Eckert DM, Kim PS (2001) Mechanisms of viral membrane fusion and its inhibition. Annu Rev Biochem 70: 777–810.
14. Lee JE, Saphire EO (2009) Ebolavirus glycoprotein structure and mechanism of entry. Future Virol 4:621–635.
15. White JM, Schornberg KL (2012) A new player in the puzzle of filovirus entry. Nat Rev Microbiol 10:317–322.
16. Harrison JS, Higgins CD, Chandran K, Lai JR (2011) Designed protein mimics of the Ebola virus glycoprotein GP2 alpha-helical bundle: Stability and pH effects. Protein Sci 20:1587–1596.
17. Root MJ, Steger HK (2004) HIV-1 gp41 as a target for viral entry inhibition. Curr Pharm Des 10:1805–1825.
18. Francis JN, Redman JS, Eckert DM, Kay MS (2012) Design of a modular tetrameric scaffold for the synthesis of membrane-localized D-peptide inhibitors of HIV-1 entry. Bioconjug Chem 23:1252–1258.
19. Dye JM, Herbert AS, Kuehne AI, Barth JF, Muhammad MA, Zak SE, Ortiz RA, Prugar LI, Pratt WD (2012) Postexposure antibody prophylaxis protects nonhuman primates from filovirus disease. Proc Natl Acad Sci USA 109:5034–5039.
20. Geisbert TW, Lee AC, Robbins M, Geisbert JB, Honko AN, Sood V, Johnson JC, de Jong S, Tavakoli I, Judge A, Hensley LE, Maclachlan I (2010) Postexposure protection of non-human primates against a lethal Ebola virus challenge with RNA interference: A proof-of-concept study. Lancet 375:1896–1905.
21. Marzi A, Feldmann H, Geisbert TW, Falzarano D (2011) Vesicular stomatitis virus-based vaccines for prophylaxis and treatment of filovirus infections. J Bioterror Biodef S1 (4).
22. Qiu X, Audet J, Wong G, Pillet S, Bello A, Cabral T, Strong JE, Plummer F, Corbett CR, Alimonti JB, Kobinger GP (2012) Successful treatment of ebola virus-infected cynomolgus macaques with monoclonal antibodies. Sci Transl Med 4:138ra181.
23. Warren TK, Warfield KL, Wells J, Swenson DL, Donner KS, Van Tongeren SA, Garza NL, Dong L, Mourich DV, Crumley S, Nichols DK, Iversen PL, Bavari S (2010) Advanced antisense therapies for post-exposure protection against lethal filovirus infections. Nat Med 16:991–994.
24. Eckert DM, Kim PS (2001) Design of potent inhibitors of HIV-1 entry from the gp41 N-peptide region. Proc Natl Acad Sci USA 98:11187–11192.
25. Eckert DM, Malashkevich VN, Hong LH, Carr PA, Kim PS (1999) Inhibiting HIV-1 entry: discovery of D-peptide inhibitors that target the gp41 coiled-coil pocket. Cell 99:103–115.
26. Eckert DM, Malashkevich VN, Kim PS (1998) Crystal structure of GCN4-pIQI, a trimeric coiled coil with buried polar residues. J Mol Biol 284:859–865.
27. Malashkevich VN, Schneider BJ, McNally ML, Milhollen MA, Pang JX, Kim PS (1999) Core structure of the envelope glycoprotein GP2 from Ebola virus at 1.9-A resolution. Proc Natl Acad Sci USA 96:2662–2667.
28. Weissenhorn W, Carfi A, Lee KH, Skehel JJ, Wiley DC (1998) Crystal structure of the Ebola virus membrane fusion subunit, GP2, from the envelope glycoprotein ectodomain. Mol Cell 2:605–616.
29. Welch BD, VanDemark AP, Heroux A, Hill CP, Kay MS (2007) Potent D-Peptide Inhibitors of HIV-1 Entry. Proc Natl Acad Sci USA 104:16828–16833.
30. Chan DC, Fass D, Berger JM, Kim PS (1997) Core structure of gp41 from the HIV envelope glycoprotein. Cell 89:263–273.
31. Weissenhorn W, Dessen A, Harrison SC, Skehel JJ, Wiley DC (1997) Atomic structure of the ectodomain from HIV-1 gp41. Nature 387:426–430.
32. Welch BD, Francis JN, Redman JS, Paul S, Weinstock MT, Reeves JD, Lie YS, Whitby FG, Eckert DM, Hill CP, Root MJ, Kay MS (2010) Design of a potent D-peptide HIV-1 entry inhibitor with a strong barrier to resistance. J Virol 84:11235–11244.
33. Salerno WJ, Seaver SM, Armstrong BR, Radhakrishnan I (2004) MONSTER: Inferring non-covalent interactions in macromolecular structures from atomic coordinate data. Nucleic Acids Res 32: W566–W568.
34. Miller MD, Geleziunas R, Bianchi E, Lennard S, Hrin R, Zhang H, Lu M, An Z, Ingallinella P, Finotto M, Mattu M, Finnefrock AC, Bramhill D, Cook J, Eckert DM, Hampton R, Patel M, Jarantow S, Joyce J, Ciliberto G, Cortese R, Lu P, Strohl W, Schleif W, McElhaugh M, Lane S, Lloyd C, Lowe D, Osbourn J, Vaughan T, Emini E, Barbato G, Kim PS, Hazuda DJ, Shiver JW, Pessi A (2005) A human monoclonal antibody neutralizes diverse HIV-1 isolates by binding a critical gp41 epitope. Proc Natl Acad Sci USA 102: 14759–14764.
35. Montgomery DL, Wang YJ, Hrin R, Luftig M, Su B, Miller MD, Wang F, Haytko P, Huang L, Vitelli S, Condra J, Liu X, Hampton R, Carfi A, Pessi A, Bianchi E, Joyce J, Lloyd C, Geleziunas R, Bramhill D, King VM, Finnefrock AC, Strohl W, An Z (2009) Affinity maturation and characterization of a human monoclonal antibody against HIV-1 gp41. MAbs 1:462–474.
36. Schumacher TN, Mayr LM, Minor DL, Jr., Milhollen MA, Burgess MW, Kim PS (1996) Identification of D-peptide ligands through mirror-image phage display. Science 271:1854–1857.
37. Weinstock MT, Francis JN, Redman JS, Kay MS (2012) Protease-resistant peptide design-empowering nature's fragile warriors against HIV. Biopolymers 98:431–442.
38. Zawadzke LE, Berg JM (1992) A racemic protein. J Am Chem Soc 114:4002–4003.
39. Dintzis HM, Symer DE, Dintzis RZ, Zawadzke LE, Berg JM (1993) A comparison of the immunogenicity of a pair of enantiomeric proteins. Proteins 16:306–308.
40. Noren KA, Noren CJ (2001) Construction of high-complexity combinatorial phage display peptide libraries. Methods 23:169–178.
41. Weinstock MT, Jacobsen MT, Kay MS (2014) Synthesis and folding of a mirror-image enzyme reveals ambidextrous chaperone activity. Proc Natl Acad Sci USA 111: 11679–11684.
42. Hackenberger CP, Schwarzer D (2008) Chemoselective ligation and modification strategies for peptides and proteins. Angew Chem Int Ed Engl 47:10030–10074.
43. Blanco-Canosa JB, Dawson PE (2008) An efficient Fmoc-SPPS approach for the generation of thioester peptide precursors for use in native chemical ligation. Angew Chem Int Edit 47:6851–6855.
44. Wan Q, Danishefsky SJ (2007) Free-radical-based, specific desulfurization of cysteine: A powerful advance in the synthesis of polypeptides and glycopolypeptides. Angew Chem Int Ed Engl 46:9248–9252.
45. Joshi SB, Dutch RE, Lamb RA (1998) A core trimer of the paramyxovirus fusion protein: parallels to influenza virus hemagglutinin and HIV-1 gp41. Virology 248:20–34.
46. Liu IJ, Kao CL, Hsieh SC, Wey MT, Kan LS, Wang WK (2009) Identification of a minimal peptide derived from heptad repeat (HR) 2 of spike protein of SARS-

CoV and combination of HR1-derived peptides as fusion inhibitors. Antiviral Res 81:82–87.
47. Wild C, Greenwell T, Matthews T (1993) A synthetic peptide from HIV-1 gp41 is a potent inhibitor of virus-mediated cell–cell fusion. AIDS Res Hum Retroviruses 9:1051–1053.
48. Watanabe S, Takada A, Watanabe T, Ito H, Kida H, Kawaoka Y (2000) Functional importance of the coiled-coil of the Ebola virus glycoprotein. J Virol 74:10194–10201.
49. Higgins CD, Koellhoffer JF, Chandran K, Lai JR (2013) C-peptide inhibitors of Ebola virus glycoprotein-mediated cell entry: Effects of conjugation to cholesterol and side chain-side chain crosslinking. Bioorgan Med Chem Lett 23:5356–5360.
50. Miller EH, Harrison JS, Radoshitzky SR, Higgins CD, Chi X, Dong L, Kuhn JH, Bavari S, Lai JR, Chandran K (2011) Inhibition of Ebola virus entry by a C-peptide targeted to endosomes. J Biol Chem 286: 15854–15861.
51. Basu A, Li B, Mills DM, Panchal RG, Cardinale SC, Butler MM, Peet NP, Majgier-Baranowska H, Williams JD, Patel I, Moir DT, Bavari S, Ray R, Farzan MR, Rong L, Bowlin TL (2011) Identification of a small-molecule entry inhibitor for filoviruses. J Virol 85: 3106–3119.
52. Roffey R, Tegnell A, Elgh F (2002) Biological warfare in a historical perspective. Clin Microbiol Infect 8:450–454.
53. Chen BK, Saksela K, Andino R, Baltimore D (1994) Distinct modes of human immunodeficiency virus type 1 proviral latency revealed by superinfection of nonproductively infected cell lines with recombinant luciferase-encoding viruses. J Virol 68:654–660.
54. Kuhn JH, Radoshitzky SR, Guth AC, Warfield KL, Li W, Vincent MJ, Towner JS, Nichol ST, Bavari S, Choe H, Aman MJ, Farzan M (2006) Conserved receptor-binding domains of Lake Victoria marburgvirus and Zaire ebolavirus bind a common receptor. J Biol Chem 281:15951–15958.
55. Connor RI, Chen BK, Choe S, Landau NR (1995) Vpr is required for efficient replication of human immunodeficiency virus type-1 in mononuclear phagocytes. Virology 206:935–944.
56. He J, Choe S, Walker R, Di Marzio P, Morgan DO, Landau NR (1995) Human immunodeficiency virus type 1 viral protein R (Vpr) arrests cells in the G2 phase of the cell cycle by inhibiting p34cdc2 activity. J Virol 69:6705–6711.
57. Deng H, Liu R, Ellmeier W, Choe S, Unutmaz D, Burkhart M, Di Marzio P, Marmon S, Sutton RE, Hill CM, Davis CB, Peiper SC, Schall TJ, Littman DR, Landau NR (1996) Identification of a major co-receptor for primary isolates of HIV-1. Nature 381:661–666.
58. Landau NR, Littman DR (1992) Packaging system for rapid production of murine leukemia virus vectors with variable tropism. J Virol 66:5110–5113.
59. Hamburger AE, Kim S, Welch BD, Kay MS (2005) Steric accessibility of the HIV-1 gp41 N-trimer region. J Biol Chem 280:12567–12572.
60. Sanchez A, Trappier SG, Mahy BW, Peters CJ, Nichol ST (1996) The virion glycoproteins of Ebola viruses are encoded in two reading frames and are expressed through transcriptional editing. Proc Natl Acad Sci USA 93:3602–3607.
61. Studier FW (2005) Protein production by auto-induction in high density shaking cultures. Protein Expr Purif 41:207–234.
62. Blommel PG, Fox BG (2007) A combined approach to improving large-scale production of tobacco etch virus protease. Protein Expr Purif 55:53–68.
63. van den Berg S, Lofdahl PA, Hard T, Berglund H (2006) Improved solubility of TEV protease by directed evolution. J Biotechnol 121:291–298.
64. Blanco-Canosa JB, Dawson PE (2008) An efficient Fmoc-SPPS approach for the generation of thioester peptide precursors for use in native chemical ligation. Angew Chem Int Ed Engl 47:6851–6855.
65. Edelhoch H (1967) Spectroscopic determination of tryptophan and tyrosine in proteins. Biochemistry 6:1948–1954.
66. Rohl CA, Baldwin RL (1997) Comparison of NH exchange and circular dichroism as techniques for measuring the parameters of the helix-coil transition in peptides. Biochemistry 36:8435–8442.
67. Cole JL (2004) Analysis of heterogeneous interactions. Methods Enzymol 384:212–232.
68. Laue T, Shah B, Ridgeway T, Pelletier S. Computer-aided interpretation of analytical sedimentation data for proteins. (1992) Analytical ultrancentrifugation in biochemistry and polymer science. Roy Soc Chem pp 90–125.
69. Wohlfarth C. Partial specific volume of poly(ethylene glycol). In: Lechner MD, Arndt KF, Eds. (2010) Polymer solutions. Berlin: Springer.
70. O'Shannessy DJ, Brigham-Burke M, Soneson KK, Hensley P, Brooks I (1993) Determination of rate and equilibrium binding constants for macromolecular interactions using surface plasmon resonance: Use of nonlinear least squares analysis methods. Anal Biochem 212:457–468.
71. Otwinowski Z, Minor W. Processing of X-ray diffraction data collected in oscillation mode. In: Carter J, CW, Sweet RM, Eds. (1997) Methods in enzymology. San Diego: Academic Press, pp 307–326.
72. McCoy AJ, Grosse-Kunstleve RW, Adams PD, Winn MD, Storoni LC, Read RJ (2007) Phaser crystallographic software. J Appl Crystallogr 40:658–674.
73. Emsley P, Cowtan K (2004) Coot: Model-building tools for molecular graphics. Acta Crystallogr D 60:2126–2132.
74. Adams PD, Afonine PV, Bunkoczi G, Chen VB, Davis IW, Echols N, Headd JJ, Hung LW, Kapral GJ, Grosse-Kunstleve RW, McCoy AJ, Moriarty NW, Oeffner R, Read RJ, Richardson DC, Richardson JS, Terwilliger TC, Zwart PH (2010) PHENIX: A comprehensive python-based system for macromolecular structure solution. Acta Crystallogr D 66:213–221.
75. Chen VB, Arendall WB, 3rd, Headd JJ, Keedy DA, Immormino RM, Kapral GJ, Murray LW, Richardson JS, Richardson DC (2010) MolProbity: All-atom structure validation for macromolecular crystallography. Acta Crystallogr D 66:12–21.
76. Jeffers SA, Sanders DA, Sanchez A (2002) Covalent modifications of the ebola virus glycoprotein. J Virol 76:12463–12472.
77. Henikoff S, Henikoff JG (1992) Amino acid substitution matrices from protein blocks. Proc Natl Acad Sci USA 89:10915–10919.

Supplementary Information

Figure S1

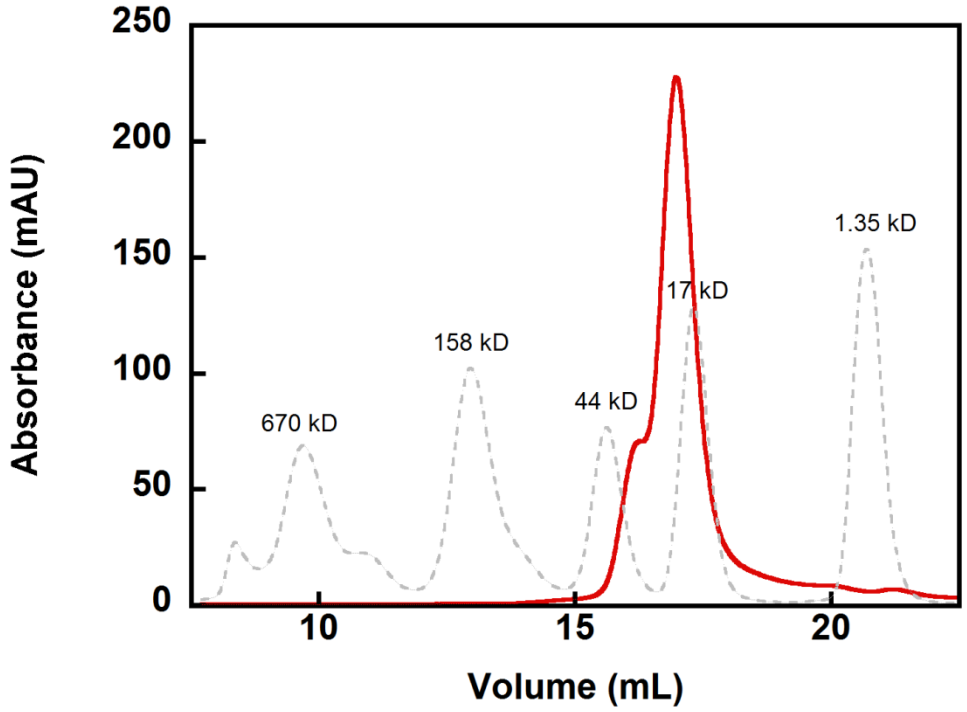

Figure S1: Gel filtration analysis of 240 µM eboIZN21 (red, recorded at 215 nm) in 50 mM sodium phosphate pH 5.8, 100 mM NaCl using a Superdex 200 column on an ÄKTApurifier (GE Healthcare Life Sciences) at room temperature with a 0.5 mL/min flowrate. Gel filtration standards (Bio-Rad) and their molecular weights are overlaid (grey, recorded at 280 nm). The predominant peak is consistent with a trimer, with a left shoulder containing higher order assemblies.

Figure S2

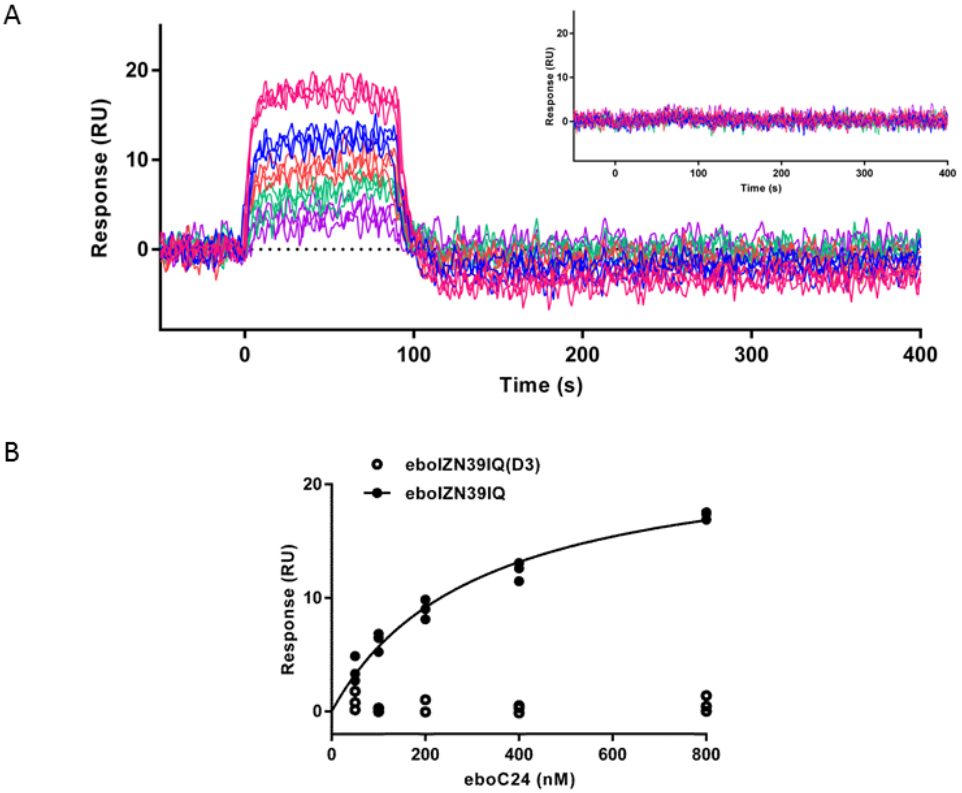

Figure S2: Binding of the ebolavirus C-peptide to the N-trimer mimic. Sensorgram of eboC24 flowed over eboIZN39IQ in a triplicate 2-fold dilution series starting at 800 nM (ProteOn XPR36, Bio-Rad), plotted with 2nd order 2-neighbor-smoothing with a Savitzky-Golay filter (Prism 6, GraphPad Software). Each dilution is shown as a distinct color. Equilibrium response data were averaged over one minute and fitted using non-linear least-squares analysis with Prism 6. The fit indicates a K_D of 310 nM. Inset: The same eboC24 dilutions flowed over an eboIZN39IQ(D3) surface. No binding was observed.

Figure S3

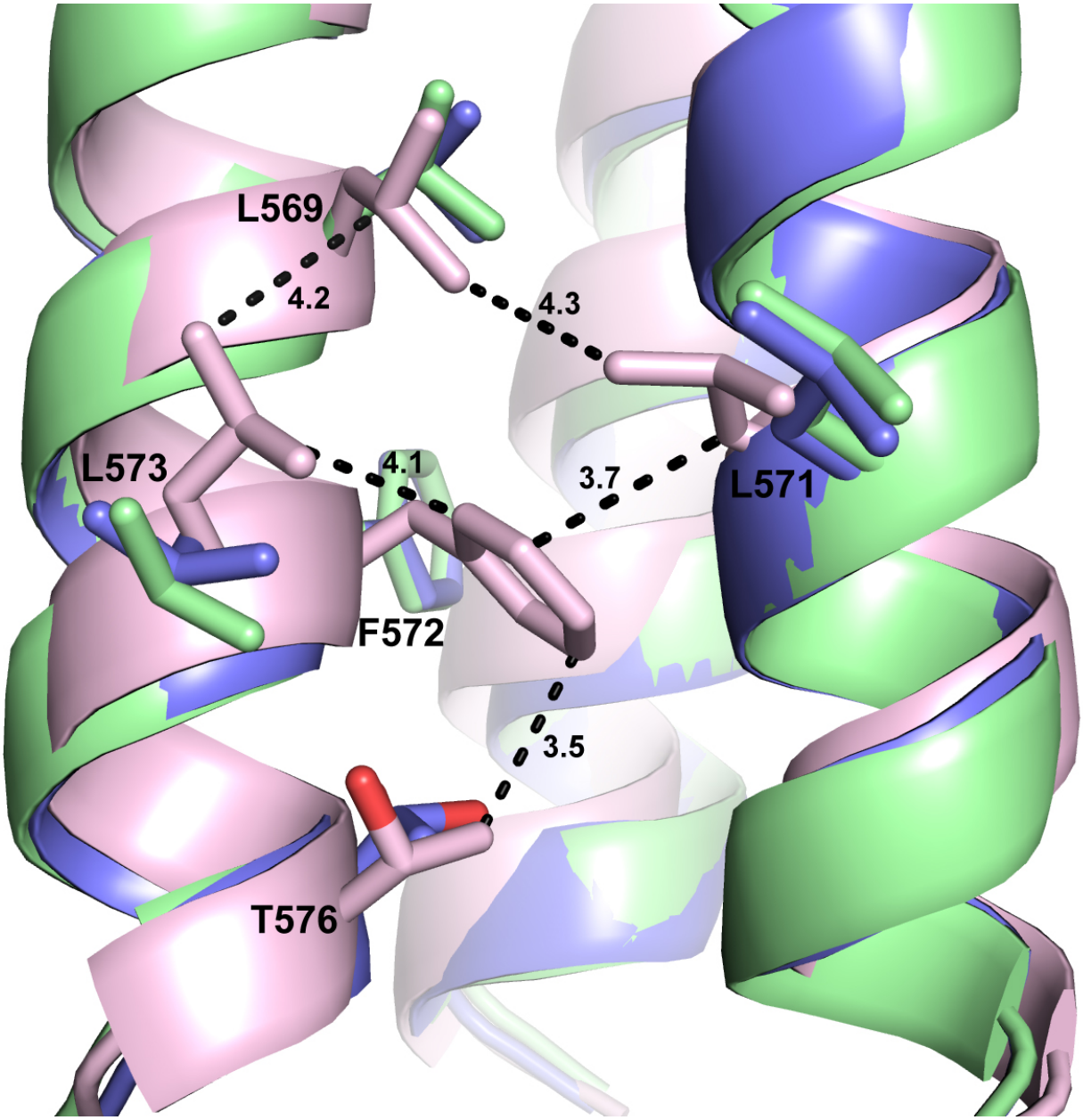

Figure S3: Hydrophobic interactions between N21 residues in the unliganded eboIZN21 structure. Shown is an overlay of the N21 region of available ebolavirus N-trimer structures in a similar view to that in Fig. 5B. Residues L569, L571, F572, L573, and T576 adopt alternate conformations in the unliganded state compared to the structures containing C-peptide and form hydrophobic interactions among themselves in the absence of ligand (dotted black lines; hydrophobic interactions for the C-peptide containing structures are not shown).

Figure S4

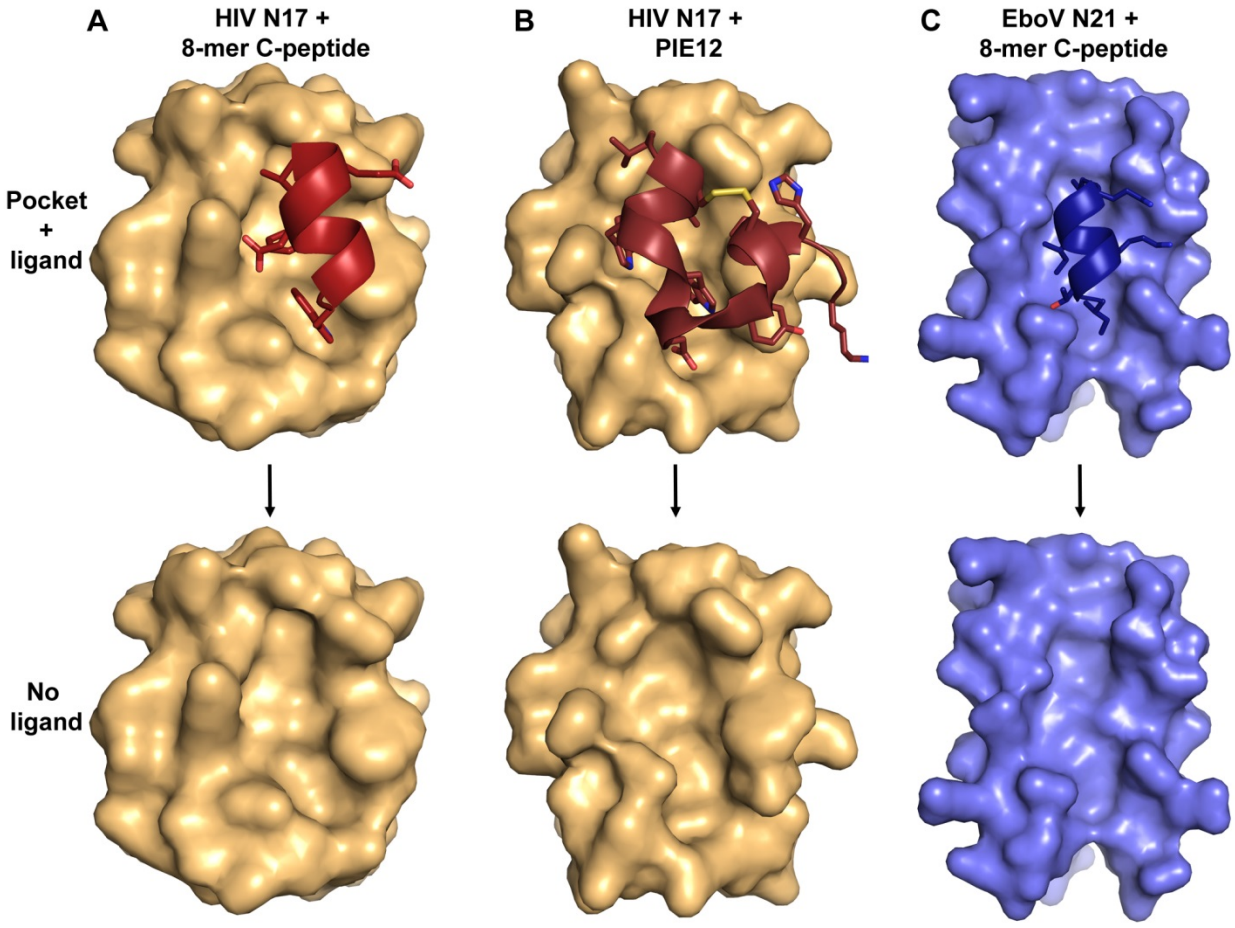

Figure S4: Comparison of hydrophobic pockets in ebolavirus and HIV N-trimers. A) Surface representation of the N17 region comprising a hydrophobic pocket in the HIV gp41 N-trimer (orange) including a cartoon representation of the eight residues (8-mer, red) of the HIV C-peptide that interact with the pocket. C-peptide residues that specifically contact pocket-forming residues are shown as sticks. The bottom panel is the same view as the top panel but without the ligand shown. B) A similar view of the HIV gp41 pocket but with the D-peptide ligand, PIE12 (dark red), bound. A comparison of the C-peptide-bound and PIE12-bound pockets indicates the shape of the pocket is ligand induced. C) A similar view of the ebolavirus N21 region (blue) from the 1EBO crystal structure showing the hydrophobic pocket with and without the 8-mer region of the ebolavirus C-peptide (dark blue) that interacts with the pocket.

Figure S5

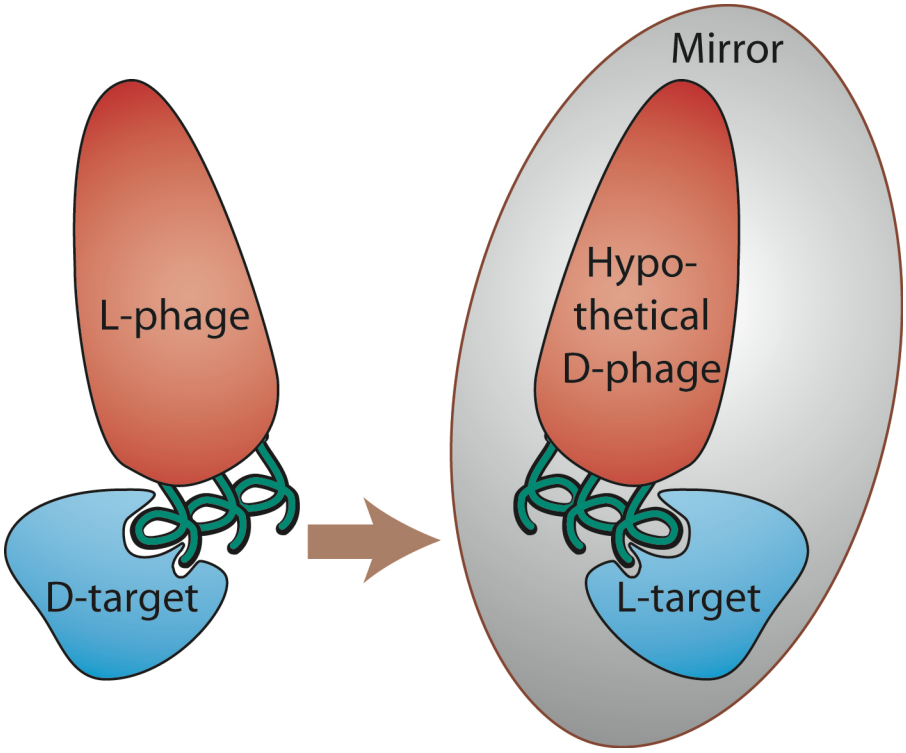

Figure S5: Mirror-Image Phage Display. In mirror-image phage display, the peptide/protein target is synthesized with D-amino acids (D-target) and forms the mirror-image of the natural L-target. Phage expressing a library of natural L-peptides (L-phage) are screened for binding to the D-target. The peptides from the specific phage clone binders are then synthesized with D-amino acids (mimicking a D-phage), and by the law of symmetry, the D-peptides will bind the natural L-target (adapted from (36)).

Figure S6

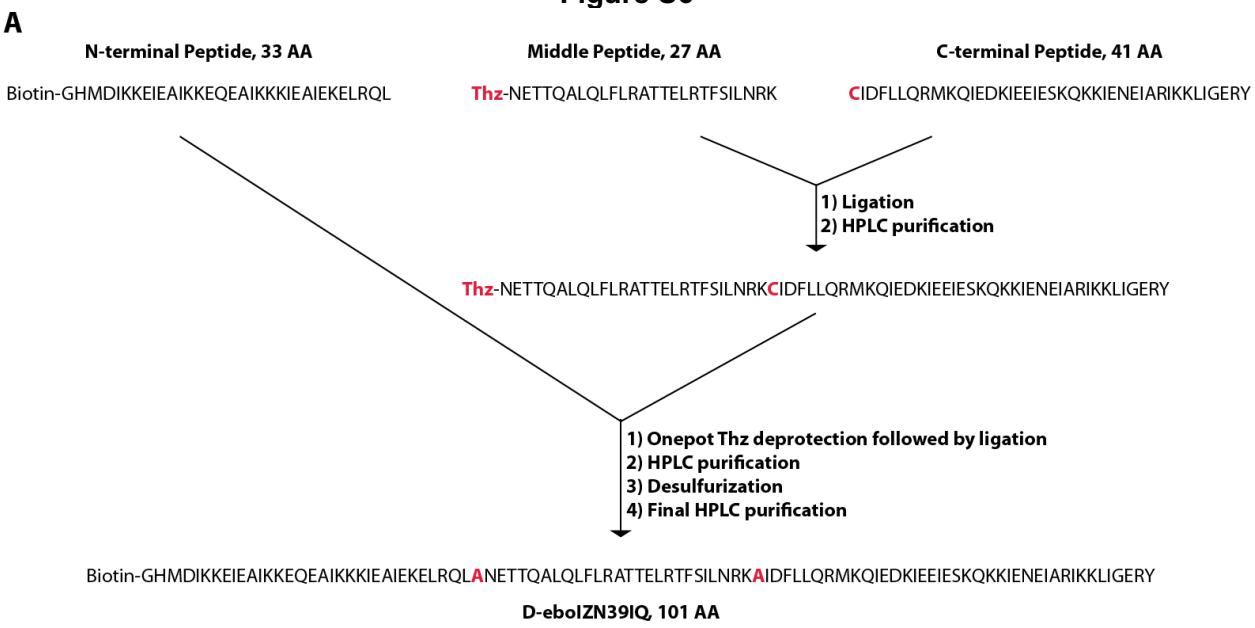

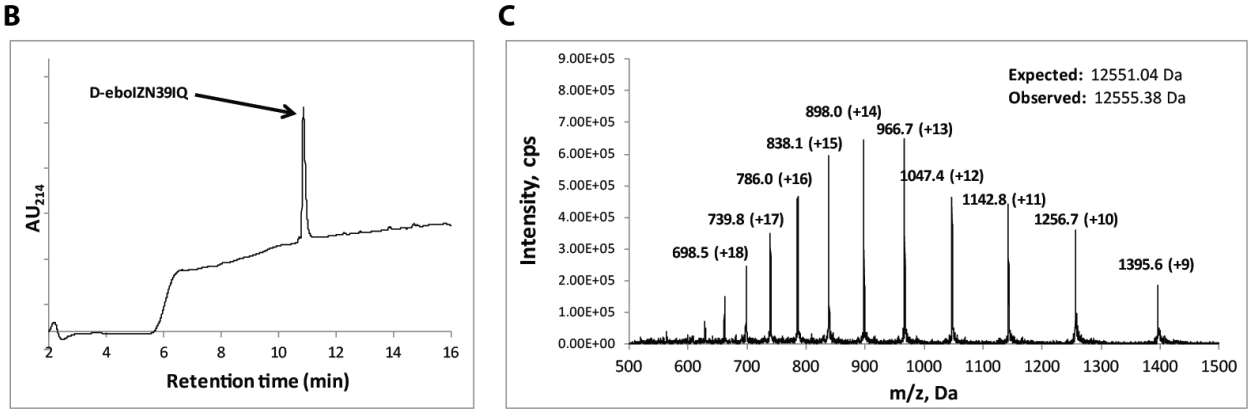

Figure S6: Synthesis of D-eboIZN39IQ. A) D-eboIZN39IQ (101 AA, with N-terminal biotin) was assembled using native chemical ligation and metal-free desulfurization. The native alanines and the residues used to replace them for native chemical ligation are indicated (red). B) HPLC analysis of final purified product D-eboIZN39IQ, using XBridge BEH130 C18 column, 2.1 x 50 mm, 5 to 90% acetonitrile gradient over 14 min, (c) MS validation showing final product with correct mass.

Figure S7

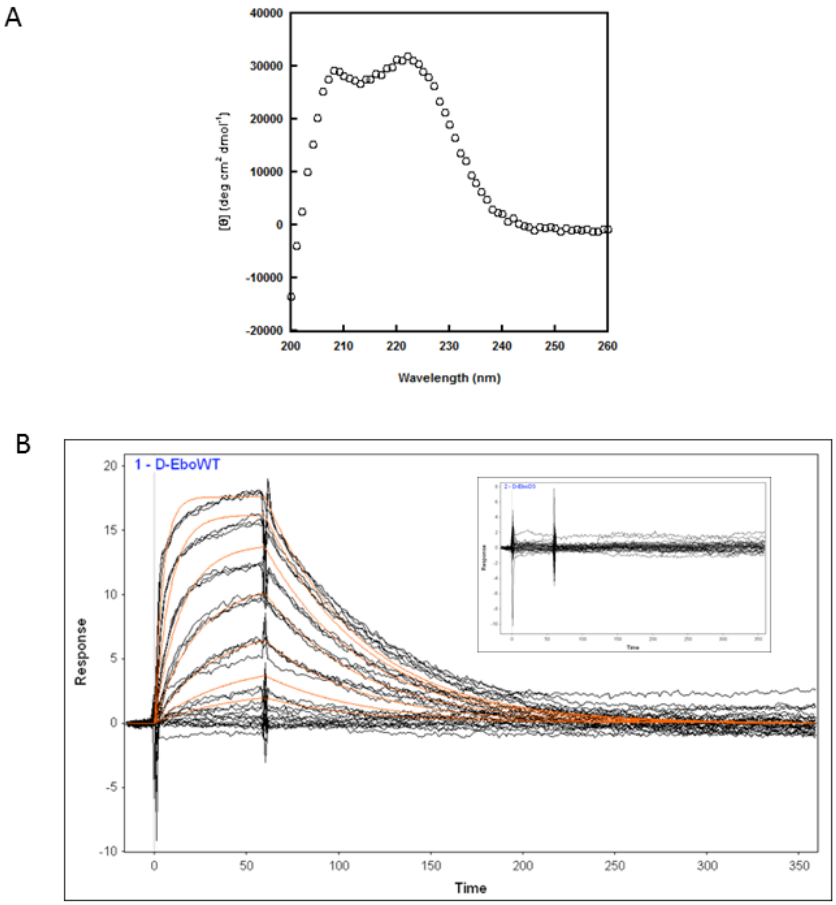

Figure S7: Biophysical characterization of the D-versions of the Ebola N-trimer mimics. A) CD spectrum of 10 μM D-eboIZN21 at 4 °C in 50 mM sodium phosphate pH 5.8, 150 mM NaCl is indicative of a highly helical conformation with 80% helicity. The positive values are as expected for this mirror-image helix. B) Analysis of binding of D-eboC37 to D-eboIZN39IQ via SPR (Biacore 3000). D-eboC37 was flowed over D-eboIZN39IQ (and D-eboIZN39IQ(D3); inset) in a 7-member 2-fold dilution series starting at 60 nM in duplicate. The fit indicates a K_D of 5.8 nM. No binding was observed to D-eboIZN39IQ(D3).

SPR methods: SPR analysis was conducted on a CM5 sensor chip (GE Healthcare) loaded with ~10,000 RU streptavidin followed by capturing ~400 RU biotin-D-eboIZN39IQ (at 40 nM in PBST* running buffer). Using Kinject, a 2-fold dilution series of D-eboC37 was flowed over the chip in duplicate at RT starting at 60 nM. A five minute dissociation time was used to ensure the response fully recovered to baseline prior to the next injection.

Table S1: ebolZN21 crystallographic data and refinement statistics

Data	
Space Group (a, b, c)	P321 (38.51, 38.51, 72.59)
Resolution (Å)	40.0 – 2.15
Resolution (Å) (high-resolution shell)	(2.23 – 2.15)
# Reflections measured	94,206
# Unique reflections	3,680
Redundancy	25.6
Completeness (%)	99.9 (99.7)
$\langle I/\sigma I \rangle$	18 (1.9)
Mosaicity (°)	0.68
Rpim[a]	0.010 (0.234)
Refinement	
Resolution (Å)	20.0 – 2.15
Resolution (Å) – (high-resolution shell)	(2.46 – 2.15)
# Reflections used for refinement	3,281
# Reflections in Rfree set	355
Rcryst[b]	0.272 (0.316)
Rfree[c]	0.294 (0.432)
RMSD: bonds (Å) / angles (°)	0.002 / 0.503
<B> (Å^2): protein atoms / # non-hydrogen atoms	63.0 / 434
<B> (Å^2): water molecules / # water molecules	59.7 / 6
ϕ/ψ most favored (%) / additionally allowed (%)	96 / 4

Values in parenthesis refer to data in the high resolution shell.

[a] Rpim = SQRT(1/N-1)*Σ|I-<I>|/ΣI where I is the intensity of an individual measurement and <I> is the corresponding mean value.

[b] Rcryst = $\Sigma||Fo|-|Fc||/\Sigma|Fo|$, where $|Fo|$ is the observed and $|Fc|$ the calculated structure factor amplitude.

[c] Rfree is the same as Rcryst calculated with a randomly selected test set of reflections that were never used in refinement calculations.